Weak Decay of Λ Hypernuclei

E. OSET[1)*] and A. RAMOS[2)†]

1) Departamento de Física Teórica and IFIC
Centro Mixto Universidad de Valencia-CSIC
46100 Burjassot (Valencia), Spain

2) Departament d'Estructura i Constituents de la Matèria
Facultat de Física, Universitat de Barcelona
08028-Barcelona, Spain

Abstract

We review recent developments concerning the weak decay of Λ hypernuclei. New studies covering the mesonic decay channel as well as recent models for the non-mesonic one are discussed and compared with experimental data. The puzzle of the neutron- to proton-induced decay ratio, Γ_n/Γ_p, is addressed in connection to the two-nucleon induced decay channel and proposals for more efficient experimental analyses of this ratio are made.

PACS: 21.80.+a, 13.30.Eg, 25.80.Pw, 13.75.Ev

Keywords: Λ hypernuclei, Mesonic decay of hypernuclei, Non-mesonic decay of hypernuclei, Weak interaction, $\Delta I = 1/2$ rule.

*e-mail: oset@evalvx.ific.uv.es
†e-mail: ramos@ecm.ub.es

Contents

1 Introduction

Hypernuclear physics is reaching the stage of a mature science. Many theoretical and experimental efforts have been devoted to the subject and a number of comprehensive reviews are already available [1, 2, 3, 4, 5, 6, 7, 8, 9, 10, 11]. The present review covers only one aspect of the investigations in the field, that of the weak decay of Λ hypernuclei. This topic has proved to be a rich one in the interface between particle and nuclear physics: both information on particle properties unaccesible with ordinary elementary reactions, as well as nuclear properties of hypernuclei, complementary to those from nuclear structure, have been obtained. Many of the interesting results from hypernuclear decay have been extensively reported in the reviews quoted above, hence the present one will be devoted essentially to the new achievements available from 1990 on.

The early experiments to produce hypernuclei using emulsions or the (K^-, π^-) reaction at CERN and BNL have given room to many new ones in a large number of experimental facilities: Σ and Λ hypernuclei have been produced at KEK using the (K^-, π) reaction with stopped kaons. The same reaction but with in-flight kaons has been studied at BNL. More recently, the (π^+, K^+) reaction at BNL and KEK has proved to be very efficient in populating deeply bound Λ states and, when studied away from the forward scattering angles, has allowed the measurement of asymmetries in the particles emitted from the decay of polarized hypernuclei. Another source of information has been obtained from LEAR, where hypernuclei and their decay are studied using $\bar{p}$ absorption followed by delayed fission. A similar technique but with protons on nuclei has been successfully developed at COSY which has allowed the measurement of lifetimes of heavy hypernuclei. The TJNAF laboratory has also joined these efforts and the $(e, e'K^+)$ reaction is now ready to produce hypernuclei with a much better energy resolution. Double strange $\Lambda\Lambda$ and Ξ hypernuclei have also been obtained from the (K^-, K^+) at BNL, opening new possibilities to the understanding of the $\Lambda\Lambda$ and ΞN interactions as well as to unravel the existence of the H particle. Finally, the FINUDA project at DAΦNE will soon use the tagged and slow K^- from the Φ decay into K^+K^- to provide data at a rate significantly higher than was available in the past.

The theoretical developments have run in parallel to the experiments. The mesonic decay of Λ hypernuclei ($\Lambda \to \pi N$) has confirmed the strong sensitivity to the pion nucleus optical potential discovered in the past. The total mesonic decay rate is significantly enhanced due to the pion interaction in the nucleus which comes, basically, from the attractive p-wave part of the optical potential. However, exclusive reactions to a final closed shell nucleus select basically the repulsive s-wave part and lead to a reduced partial decay rate. The simultaneous study of inclusive and exclusive decay reactions can thus be a good source of information on the pion nucleus interaction, complementary to the one obtained from pionic atoms and low energy pion nucleus scattering. The mesonic decay of light hypernuclei has provided evidence of the strong repulsion of the ΛN interaction at short distances, a property that follows naturally from available quark models of the strong YN interaction.

The non-mesonic decay mode ($\Lambda N \to NN$) has received much attention and

detailed models which go beyond the original one pion exchange mechanism are now available, either including the exchange of several mesons or working explicitly in terms of the quark degrees of freedom. One of the motivations for developing these models was the large discrepancies between theory and experiment in the ratio Γ_n/Γ_p of neutron- to proton-stimulated non-mesonic decay, where the one pion model seems to provide an order of magnitude smaller ratio than the data. The question is not yet settled but one of the things that has been recently found is that the consideration of the two-nucleon-induced decay mode ($\Lambda NN \to NNN$) enlarges the error bars from present experimental analyses. The two-nucleon-induced non-mesonic decay of Λ hypernuclei was considered with the hope that it could solve the Γ_n/Γ_p puzzle. While it has been seen that this is not the case, the new decay remains, however, as a channel which must be taken into account in any attempt of a precise analysis of the experimental data. Theoretical studies of the neutron and proton spectra from the decay of Λ hypernuclei are now available and open new doors for a more reliable determination of the Γ_n/Γ_p ratio than was possible in the past.

In this review we concentrate only on the weak decays of Λ hypernuclei. The progress in Σ hypernuclei has been scarce both experimentally and theoretically, however, the narrow Σ states claimed by old spectra have not been observed in a recent experiment carried out at BNL with better statistics. Another interesting experiment has been the clean measurement of the ${}^{4}_{\Sigma}$He hypernucleus at BNL [12], giving stronger grounds for the existence and properties of this state than the previous findings at KEK using stopped kaons. Also, the availability of $\Lambda\Lambda$ and Ξ hypernuclei has stimulated many theoretical studies aimed at obtaining information about the $\Lambda\Lambda$ and ΞN interaction. A comprehensive recent review on these latter issues can be found in ref. [11].

2 Weak mesonic decay of hypernuclei

2.1 Derivation of the Λ width in nuclei

We make here a formal derivation of the width of Λ states bound in nuclei. In the first place we evaluate the Λ width for a Λ particle moving through infinite nuclear matter. The width for finite nuclei is obtained from there using the local density approximation (LDA). In a second step we follow a direct approach to the evaluation of the Λ mesonic width in finite nuclei and compare the methods. Anticipating results we find that the nuclear matter plus LDA is a good tool to evaluate Λ decay widths in nuclei. For the non-mesonic channel, where the energy carried by the emitted nucleons is large, the LDA predicts decay rates within 5% of the finite nuclei results. The mesonic width is more sensitive to nuclear shell effects given the little phase space available for the reaction. In medium hypernuclei around ${}^{12}_{\Lambda}$C, assuming one uses the correct Q value of the reaction, one may expect the LDA results to lie within 20–30 % of the correct answer. In lighter hypernuclei the mesonic width approaches gradually the free one and the uncertainties naturally diminish. In heavier hypernuclei, where the mesonic rate is reduced in several orders of magnitude, the errors are larger. In this case the LDA can only account qualitatively for the mesonic width, however it provides the essential features of the reaction, such as the reduction in the rate with increasing mass of the hypernucleus, as well as the dramatic increase of the rate due to the pion interaction with the nucleus.

We also discuss here two ways of evaluating the decay process, one by means of Feynman diagrammatic technique and the use of meson and nucleon propagators, the other one that uses operators and wave functions and we show the equivalence of the two methods.

2.1.1 The propagator method

The starting point is the $\Lambda \longrightarrow \pi N$ Lagrangian, accounting for this weak process, which is given by

$$\mathcal{L}^{\rm W}_{\Lambda {\rm N}\pi} = -iG_F\mu^2\overline{\psi}_{\rm N}(A_\pi + B_\pi\gamma_5)\vec{\tau}\vec{\phi}_\pi\psi_\Lambda \begin{pmatrix}0\\1\end{pmatrix} + {\rm h.c.}\ , \tag{1}$$

where $G_F\mu^2 = 2.21\times 10^{-7}$ is the weak coupling constant. The empirical constants $A_\pi = 1.05$ and $B_\pi = -7.15$, adjusted to the observables of the free Λ decay, determine the strength of the parity violating and parity conserving amplitudes, respectively. The nucleon, Λ and pion fields are given by $\psi_{\rm N}$, ψ_Λ and $\vec{\phi}_\pi$, respectively, while the isospin spurion $\binom{0}{1}$ is included to enforce the empirical $\Delta I = 1/2$ rule, according to which the strength for the $\Lambda \to \pi^- p$ decay is double than that for $\Lambda \to \pi^0 n$.

A practical way to evaluate the Λ width in nuclear matter and to introduce medium corrections is to start from the Λ self-energy, Σ, associated to the diagram of fig. 1, and then use the relationship

$$\Gamma = -2{\rm Im}\,\Sigma. \tag{2}$$

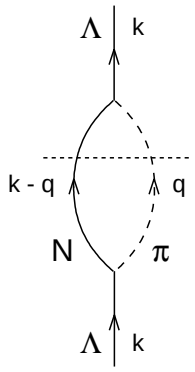

Figure 1: Feynman graph for the free Λ self-energy of eq. (3). The $\Lambda \to \pi N$ "cut" is shown (dotted line).

Following standard Feynman rules, and making a non relativistic reduction of the operators in eq. (1), the self-energy is readily evaluated as

$$-i\Sigma(k) = 3(G_F\mu^2)^2 \int \frac{d^4q}{(2\pi)^4} G(k-q)D(q) \left[S^2 + \left(\frac{P}{\mu}\right)^2 \vec{q}^{\,2} \right] , \tag{3}$$

where G and D are the nucleon and pion propagators, respectively, $S = A_\pi$, and $P/\mu = B_\pi/2M$ with μ and M the pion and nucleon masses.

The free nucleon and pion propagators are given respectively by

$$\begin{aligned} G(k) &= \frac{1}{k^0 - E(\vec{k}) + i\epsilon} \\ D(q) &= \frac{1}{q^{0\,2} - \vec{q}^{\,2} - \mu^2 + i\epsilon} , \end{aligned} \tag{4}$$

where the typical nonrelativistic approximations are done in the nucleon propagator: only the positive energy part of the nucleon propagator is taken and the factor M/E (E being the relativistic energy) is set equal to unity.

By using the free nucleon and pion propagators one obtains immediately the free Λ width [5, 13]

$$\begin{aligned} \Gamma_{\rm free} \equiv \Gamma_\Lambda &= 3(G_F\mu^2)^2 \int \frac{d^3q}{(2\pi)^3} \frac{1}{2\omega(\vec{q})} 2\pi\delta(E_\Lambda - \omega(q) - E(\vec{k}-\vec{q})) \\ &\quad \times \left[S^2 + \left(\frac{P}{\mu}\right)^2 \vec{q}^{\,2} \right] , \end{aligned} \tag{5}$$

where $E_\Lambda, \omega(q), E(\vec{k}-\vec{q})$ are the energies of the Λ, pion and nucleon, respectively.

In a Fermi sea of nucleons, both the nucleon and pion propagators are changed to

$$G(p) = \frac{1 - n(\vec{p})}{p^0 - E(\vec{p}) - V_N + i\epsilon} + \frac{n(\vec{p})}{p^0 - E(\vec{p}) - V_N - i\epsilon} \tag{6}$$

$$D(q) = \frac{1}{q^{0\,2} - \vec{q}^{\,2} - \mu^2 - \Pi(q^0, \mathrm{q})} \ , \tag{7}$$

where V_N is the nucleon potential, $\Pi(q^0, \mathrm{q} = \mid \vec{q} \mid)$ is the pion self-energy in the nuclear medium and $n(\vec{p})$ is the occupation number in the Fermi sea, $n(\vec{p}) = 1$ for $|\vec{p}| \leq k_F$ and $n(\vec{p}) = 0$ for $|\vec{p}| > k_F$, with k_F the Fermi momentum. An appropriate choice for V_N is the Thomas Fermi potential, $V_N = -k_F^2/2M$, which becomes $\vec{r}$ dependent when the local Fermi momentum $k_F(r) = (\frac{3}{2}\pi^2\rho(r))^{1/3}$ is used.

The practical way to perform the q^0 integral in eq. (3) is through the Wick rotation displayed in fig. 2, where the analytical structure of the integrand is shown. The shaded region accounts for the discontinuity of the pion propagator due to $\mathrm{Im}\,\Pi$. In [13] one includes particle-hole (ph) and Δ-hole (Δh) excitation as a source of the p-wave pion self-energy plus and extra s-wave self-energy. Coulomb effects are neglected. Thus

$$\begin{aligned} \Pi(q) &= \Pi^{(s)}(q) + \vec{q}^{\,2}\tilde{\Pi}(q) \\ \text{with} \quad \tilde{\Pi}(q) &= \frac{\dfrac{f^2}{\mu^2}U(q)}{1 - g'\dfrac{f^2}{\mu^2}U(q)} \\ \text{and} \quad U(q) &= U_N(q) + U_\Delta(q) \ . \end{aligned} \tag{8}$$

In eq. (8), $U(q)$ is the Lindhard function which gets strength from ph excitation, $U_N(q)$, and Δh excitation, $U_\Delta(q)$, and g' is the Landau-Migdal parameter. In the Λ decay case, $U_N(q)$ has both real and imaginary parts, the latter one due to those contributions in the integration over the internal variables for which the ph excitation appears on the mass shell. The function $U_\Delta(q)$ has also real and imaginary parts, the latter one coming from the (energy dependent) Δ width, which is relatively small in the Λ decay case since the pions emerge with little energy. Then, for practical purposes one can neglect $\mathrm{Im}\,U_\Delta$. In this case, the analytical structure of the integrand in eq. (3) with the medium propagators (6) and (7) shows, in addition to the cut (region of discontinuity in the real axis due to $\mathrm{Im}\,U_N \neq 0$), a pole in $q^0 = \tilde{\omega}(\vec{q})$ corresponding to a renormalized pion energy for which

$$\tilde{\omega}(\vec{q})^2 - \vec{q}^{\,2} - \mu^2 - \Pi(\tilde{\omega}(\vec{q}), \mathrm{q}) = 0 \ . \tag{9}$$

Missing in fig. 2 is the pole of $G(\vec{k} - \vec{q})$ corresponding to the second term in eq. (6). This pole lies in the lower half-plane of the figure and would contribute in the Wick rotation only when it happens to be in the third quadrant, i.e., $k^0 - E(\vec{k} - \vec{q}) - V_N < 0$. But this corresponds to $(\vec{k} - \vec{q})$ very large where $n(\vec{k} - \vec{q}) = 0$ and hence this term does not contribute.

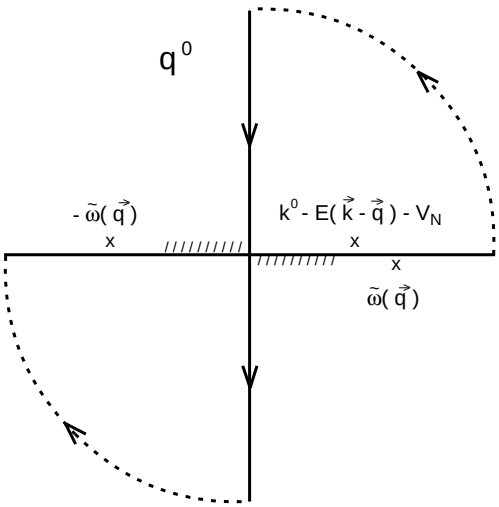

Figure 2: Analytical structure of the integrand of eq. (3) in the complex q^0 plane with the nucleon and pion propagators of eqs. (6), (7). The renormalized pion propagator pole $\tilde{\omega}(q)$ is shown. The dashed lines close to the real axis indicate the analytical cut from $\mathrm{Im}\,\Pi(q^0, q)$ related to the non-mesonic Λ decay channel.

We come back to the evaluation of $\Sigma(k)$ in the nuclear medium, eq. (3), using the nucleon and pion propagators of eqs. (6) and (7). In the integral over q^0 along the contour of fig. 2, the contributions of the arcs at infinity vanish and the integral along the imaginary axis contributes only to $\mathrm{Re}\,\Sigma$, given the property of the integrand $I(q^0) = I^*(q^{0*})$. Thus, only the residue of the integrand at the pole of the first quadrant is responsible for $\mathrm{Im}\,\Sigma$ and we obtain for the width [5, 13]

$$\begin{aligned}\Gamma(k) &= -6(G_F\mu^2)^2 \int \frac{d^3q}{(2\pi)^3}[1 - n(\vec{k}-\vec{q})]\theta(k^0 - E(\vec{k}-\vec{q}) - V_N) \\ &\times \left[S^2 + \left(\frac{P}{\mu}\right)^2 \vec{q}^{\,2}\right] \mathrm{Im}\ \frac{1}{q^{0\,2} - \vec{q}^{\,2} - \mu^2 - \Pi(q^0, \mathrm{q})}\bigg|_{q^0 = k^0 - E(\vec{k}-\vec{q}) - V_N} . \quad (10)\end{aligned}$$

In the discussion here we neglect the role of correlations and form factors, which are important only in the non-mesonic decay. We shall discuss this in detail when studying this decay mode in Sect. 3.

In eq. (10) we observe the Pauli blocking factor, $1-n$. Since a Λ with momentum $\vec{k} = 0$ decays into a nucleon and pion with q $\simeq$ 100 MeV/c, this momentum is smaller than the Fermi momentum for nuclear matter density, $k_F = 270$ MeV/c, and the decay is forbidden by Pauli blocking, i.e, $1 - n(\vec{k} - \vec{q}) = 0$. In finite nuclei it is still possible to have mesonic decay since the Λ wave function has some overlap with the nuclear surface where the Fermi momentum will be smaller than 100 MeV/c.

Moreover, the momentum distribution of the Λ leads to some spreading in the nucleon momenta allowing some of them to overcome the Pauli blocking. Nevertheless, the Λ mesonic width decreases drastically as a function of the mass number.

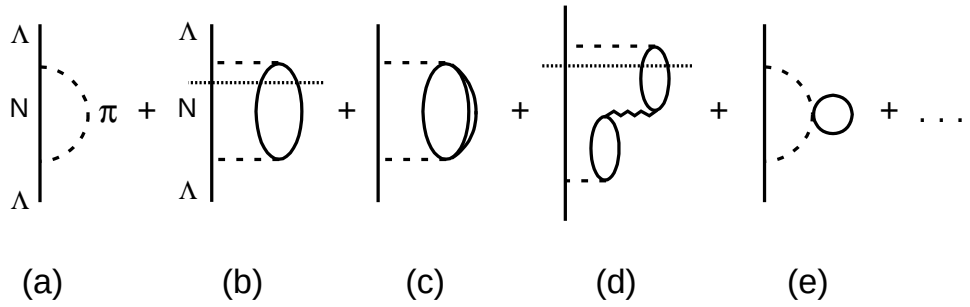

Figure 3: Λ self-energy diagrams included in eq. (3) with the nucleon and pion propagators of eqs. (6), (7). (a) Free self-energy graph. (b), (c) Insertion of p-wave pion self-energy at lowest order. (d) Generic RPA graph from the expansion of the pion propagator in powers of the pion self-energy. (e) s-wave pion self-energy at lowest order. The cuts represent the non-mesonic decay channel.

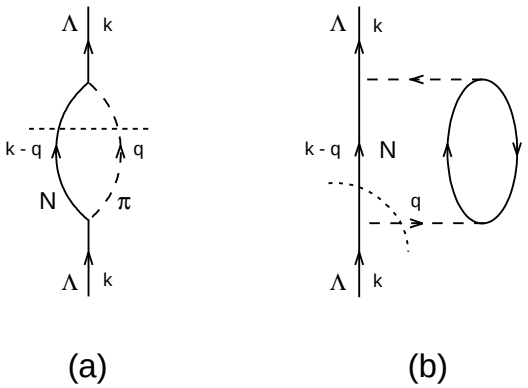

Figure 4: Free and lowest order Λ self-energy graph. The dotted cuts represent the mesonic decay channel.

The language of propagators used here is very adequate to provide a unified picture of the Λ nuclear decay. Indeed, eq. (10) contains not only the modified mesonic channel but also the non-mesonic one. This can be seen diagrammatically by expanding the pion propagator and taking a ph and Δh excitation to account for the pion self-energy, Π. This is depicted in fig. 3. The imaginary part of a self-energy diagram is obtained when the set of intermediate states cut by a horizontal line are

placed simultaneously on shell in the intermediate integration. In fig. 3 we observe a source corresponding to placing on shell a nucleon and the ph of the pion self-energy. This corresponds to a channel where there are no pions and only nucleons in the final state. The physical process which has occurred is $\Lambda N \to NN$, which corresponds to the standard non-mesonic channel. Technically, it would be obtained by substituting in eq. (10)

$$\mathrm{Im}\,\frac{1}{q^{0\,2}-\vec{q}^{\,2}-\mu^2-\Pi} \longrightarrow \frac{\mathrm{Im}\,\Pi_{ph}}{|q^{0\,2}-\vec{q}^{\,2}-\mu^2-\Pi|^2}\ , \tag{11}$$

where Π_{ph} is the pion self-energy due to ph excitations. There is no overlap between $\mathrm{Im}\,\Pi_{ph}(q^0,\mathrm{q})$ and the pion pole in the propagator of eq. (10) and thus the separation of the mesonic and non-mesonic channels can be done in a clean way.

The mesonic channel would correspond to a different cut, the one where the N and the π are placed on shell. This is shown in fig. 4, where the diagram of fig. 4(a) corresponds to the lowest order in the expansion of the pion propagator. This term, together with the one in fig. 4(b) and further iterations contained in eq. (10), lead to a renormalization of the mesonic width, and an appreciable one, as it was shown in ref. [13].

Technically, the mesonic width can be calculated either by subtracting the non-mesonic width from the total width, eq. (10), or, equivalently, by replacing the pion pole contribution in eq. (5) by the renormalized pion pole given in eq. (9). In this latter case the mesonic width is obtained, by analogy to eq. (5), from

$$\begin{aligned}\Gamma_\pi &= 3(G_F\mu^2)^2\int\frac{d^3q}{(2\pi)^3}\frac{1}{\left|2\tilde{\omega}(\vec{q})-\frac{\partial\Pi}{\partial\tilde{\omega}}\right|}2\pi\delta(E_\Lambda-\tilde{\omega}(\vec{q})-E(\vec{k}-\vec{q})-V_N)\\ &\quad\times\left[S^2+\left(\frac{P}{\mu}\right)^2\vec{q}^{\,2}\right]\ .\end{aligned} \tag{12}$$

The qualitative reason for the drastic change on the mesonic width is given in [5,13]: the attractive character of the pion self-energy leads to a larger pion momentum for the same pion energy and thus, to a larger nucleon momentum by momentum conservation. Thus, the nucleon has more chances to have a momentum bigger than the Fermi momentum, therefore increasing the mesonic width.

The width in finite nuclei is obtained in [13] via the LDA

$$\Gamma=\int d^3r|\phi_\Lambda(\vec{r})|^2\Gamma(k,\rho(\vec{r}))\ , \tag{13}$$

where ϕ_Λ is the Λ wave function. A further average over the momentum distribution of the Λ wave function is also done in [13].

2.1.2 Finite nuclei approach. The wave function method

The finite nuclei approach to the mesonic width was sketched in [14] and carried out in detail in [15]. The mesonic width is given, in analogy to eq. (5), by

$$\Gamma^{(\alpha)} = \frac{1}{2}C^{(\alpha)}(G_F\mu^2)^2\sum_{N\notin F}\int\frac{d^3q}{(2\pi)^3}\frac{1}{2\omega(\vec{q})}2\pi\delta(E_\Lambda-\omega(\vec{q})-E_N)$$

$$\times \left\{ S^2 \left| \int d^3x \phi_\Lambda(\vec{x}) \phi_\pi^{(-)}(\vec{q},\vec{x})^* \phi_N^*(\vec{x}) \right|^2 \right.$$
$$\left. + \left(\frac{P}{\mu}\right)^2 \left| \int d^3x \phi_\Lambda(\vec{x}) \vec{\nabla} \phi_\pi^{(-)}(\vec{q},\vec{x})^* \phi_N^*(\vec{x}) \right|^2 \right\} , \quad (14)$$

where ϕ_N is the wave function of the nucleon states and $\phi_\pi^{(-)*}$ corresponds to an outgoing solution of the Klein Gordon equation normalized to a plane wave asymptotically ($e^{-i\vec{q}\vec{x}}$). The index α stands now for $\pi^- p$ or $\pi^0 n$ decay, with $C^{(p)} = 4, C^{(n)} = 2$, which one separates here since, due to shell effects, these channels can depart drastically from the elementary $\Delta I = 1/2$ rule.

The sum in eq. (14) runs only over non occupied nucleon states in the shell model. On the other hand, $\phi_\pi^{(-)*}$ is a solution of the Klein Gordon equation with a proper optical potential (or pion self-energy, $\Pi = 2\omega V_{opt}$), including Coulomb effects through V_c, i.e.,

$$\left[-\vec{\nabla}^2 + \mu^2 + 2\omega V_{opt}(\vec{x}) \right] \phi_\pi^{(-)}(\vec{q},\vec{x})^* = \left[\omega - V_c(\vec{x}) \right]^2 \phi_\pi^{(-)}(\vec{q},\vec{x})^* \ . \quad (15)$$

The effects of using $\phi_\pi^{(-)*}$ instead of a plane wave are rather drastic and increase the mesonic width in about two orders of magnitude in heavy nuclei [15, 16, 17], in qualitative agreement with the nuclear matter results of ref. [13].

The arguments for the renormalization are expressed now in the alternative language as follows: the attraction caused by the pion self-energy leads to higher momentum components in the pion wave function and, as a consequence, the matrix element of eq. (14), which involves the Λ wave function in the $1s_{1/2}$ ground state and a nucleon wave function in an unoccupied orbit, is considerably enhanced. To see this let us write the pion wave function in terms of its Fourier transform

$$\phi_\pi^{(-)}(\vec{q},\vec{x})^* = \int d^3q' e^{-i\vec{q}'\vec{x}} \tilde{\phi}_\pi(\vec{q},\vec{q}') \ ,$$

and recall that for $| \vec{x} | \to \infty$ it behaves as $e^{-i\vec{q}\vec{x}}$. For values of $\vec{x}$ inside the nucleus, due to the attractive character of the pion nucleus potential, the pion wave function builds up $\vec{q}'$ momentum components such that $| \vec{q}' | > | \vec{q} |$. Then, the strength of the transition, $| \langle N | e^{-i\vec{q}'\vec{x}} \simeq 1 - i\vec{q}'\vec{x} - (\vec{q}'\vec{x})^2/2 + \ldots | \Lambda \rangle |$, appearing in eq. (14), is governed by the momentum $\vec{q}'$ which, being larger in magnitude than $\vec{q}$, leads to enhanced matrix elements with respect to those using the asymptotic free pion wave. In the two languages the physical consequences are the same: an increased probability of reaching the unoccupied states and thus an enhancement of the mesonic width.

2.1.3 Equivalence of the propagator and wave function methods

Even if apparently the two methods discussed above look quite different, the physics contained in the propagator and wave function methods is equivalent. A formal derivation of the connection between the methods can be found in [18], which we reproduce here for completeness, complementing some points concerning the pion propagator in infinite nuclear matter and finite nuclei .

Let us start from the pion propagator in finite nuclei written in coordinate space

$$D(\vec{x},\vec{y},\omega)=\sum_n \frac{\phi_n(\vec{x})\phi_n^*(\vec{y})}{\omega^2-\epsilon_n^2+i\eta}\ , \tag{16}$$

where $\phi_n(\vec{x})$ are the pion wave functions in the nucleus and ϵ_n their corresponding energies. Ignoring pionic bound states, which do not play a role in our problem, we can identify the pionic wave functions by the asymptotic momentum $\vec{q}$. Hence their energy is given by $\omega(\vec{q})=(\vec{q}^2+\mu^2)^{1/2}$. The sum over the index n is then replaced by an integral over $\vec{q}$ as given below

$$D_\pi(\vec{x}_1,\vec{x}_2;E_\pi)=\int \frac{d^3q}{(2\pi)^3}\frac{\phi_\pi(\vec{q},\vec{x}_1)\phi_\pi^*(\vec{q},\vec{x}_2)}{E_\pi^2-\omega(\vec{q})^2+i\eta}\ . \tag{17}$$

For simplicity in the derivation we shall take the parity violating part of the width (the one providing the largest contribution to the mesonic decay) and will not distinguish between π^0 or π^- decay. Hence, from eq. (14) we obtain

$$\begin{aligned}\Gamma_S &= 3(G_F\mu^2)^2S^2\sum_{N\notin F}\int\frac{d^3q}{(2\pi)^3}\frac{1}{2\omega(\vec{q})}2\pi\delta(E_\Lambda-E_N-\omega(\vec{q}))\\ &\quad\times\left|\int d^3x\phi_\Lambda(\vec{x})\phi_\pi^*(\vec{q},\vec{x})\phi_N^*(\vec{x})\right|^2\ ,\end{aligned} \tag{18}$$

which can be rewritten as

$$\begin{aligned}\Gamma_S &= 3(G_F\mu^2)^2S^2\int d^3x_1\int d^3x_2\phi_\Lambda^*(\vec{x}_1)\phi_\Lambda(\vec{x}_2)\phi_N(\vec{x}_1)\phi_N^*(\vec{x}_2)\\ &\times\ \int\frac{d^3q}{(2\pi)^3}\frac{1}{2\omega(\vec{q})}2\pi\delta(E_\Lambda-E_N-\omega(\vec{q}))\phi_\pi(\vec{q},\vec{x}_1)\phi_\pi^*(\vec{q},\vec{x}_2)\ ,\end{aligned} \tag{19}$$

or, by virtue of eq. (17), as

$$\begin{aligned}\Gamma_S &= 3(G_F\mu^2)^2S^2\sum_{N\notin F}\int d^3x_1d^3x_2\phi_\Lambda^*(\vec{x}_1)\phi_N(\vec{x}_1)(-2)\mathrm{Im}\,D_\pi(\vec{x}_1,\vec{x}_2;E_\pi=E_\Lambda-E_N)\\ &\quad\times\theta(E_\Lambda-E_N)\phi_\Lambda(\vec{x}_2)\phi_N^*(\vec{x}_2)\ .\end{aligned} \tag{20}$$

Now, in order to connect with eqs. (10) and (13) one makes a local density approximation. In the first step one evaluates Γ for a slab of infinite nuclear matter and in the second step one replaces the width in the infinite slab by an integral over the nuclear volume assuming slabs of matter in each d^3r of the nucleus with local density $\rho(\vec{r})$ and with a probability of finding the Λ particle given by $|\phi_\Lambda(\vec{r})|^2$. This last step is implemented by means of eq. (13). Hence we should see how we reproduce now eq. (10) when we assume in eq. (20) a slab of infinite nuclear matter. For this purpose we have to replace for the nucleon sector

$$\sum_{N\notin F}\to V\int\frac{d^3p}{(2\pi)^3}(1-n(\vec{p}))$$

$$\phi_N(\vec{x}) \to \frac{1}{\sqrt{V}} \mathrm{e}^{i\vec{p}\vec{x}}$$

$$E_N \to E(\vec{p}) - V_N \ , \tag{21}$$

and for the Λ wave function

$$\phi_\Lambda(\vec{x}) \to \frac{1}{\sqrt{V}} \mathrm{e}^{i\vec{k}\vec{x}} \ . \tag{22}$$

Now, in the infinite slab of nuclear matter the pion propagator of eq. (17) is replaced by

$$D_\pi(\vec{x}_1, \vec{x}_2, E_\pi) \to \int \frac{d^3q}{(2\pi)^3} \frac{\mathrm{e}^{i\vec{q}(\vec{x}_1 - \vec{x}_2)}}{E_\pi^2 - \omega(\vec{q})^2 - \Pi(E_\pi, \vec{q})} \ , \tag{23}$$

where $\Pi(E_\pi, \vec{q})$ is the pion self-energy, which is a function of ρ. Note that for values of $\vec{x}_1, \vec{x}_2$ far away from the nucleus, eqs. (17) and (23) are equivalent since there $\rho = 0$ and Π (in the LDA) will be zero. At other densities, Π will be different from zero and the integral of eq. (23) gives rise to other momentum components, modulating the plane wave in the numerator and providing a kind of WKB approximation to the wave functions in the numerator of eq. (17). The LDA gives rise to a variable local momentum and hence a distorted pion wave.

By substituting eqs. (21), (22), (23) in eq. (20) we obtain:

$$\begin{aligned} \Gamma_S &= -6(G_F\mu^2)^2 S^2 \int \frac{d^3p}{(2\pi)^3} \int \frac{d^3q}{(2\pi)^3} (1 - n(\vec{p})) \mathrm{Im}\, D_\pi(q) \theta(q^0) \Big|_{q^0 = E_\Lambda - E(\vec{k} - \vec{q}) - V_N} \\ &\quad \times \int d^3x_1 d^3x_2 \frac{1}{V} \mathrm{e}^{i\vec{p}(\vec{x}_1 - \vec{x}_2)} \mathrm{e}^{i\vec{q}(\vec{x}_1 - \vec{x}_2)} \mathrm{e}^{-i\vec{k}(\vec{x}_1 - \vec{x}_2)} \ , \end{aligned} \tag{24}$$

with $D_\pi(q)$ given by eq. (7). Finally, by means of the relationship $(2\pi)^3 \delta^3(0) = \int d^3x = V$ we can cast eq. (24) as

$$\Gamma_S = -6(G_F\mu^2)^2 S^2 \int \frac{d^3q}{(2\pi)^3} (1 - n(\vec{k} - \vec{q})) \mathrm{Im}\, D_\pi(q) \theta(q^0) \Big|_{q^0 = E_\Lambda - E(\vec{k} - \vec{q}) - V_N} \ , \tag{25}$$

which coincides with the s-wave contribution to Γ from eq. (10). This establishes the equivalence between the finite nuclei wave functions method and the propagator method, the latter one complemented with the LDA.

A further consideration can be done regarding the pion propagators in finite nuclei and nuclear matter, eqs. (17) and (23) respectively. Neglecting, for simplicity, the Coulomb potential, assuming a smooth energy dependence of the pion self-energy and taking Π for a value of E_π around the pion pole, the Klein-Gordon equation leads to

$$\begin{aligned} \left[-\vec{\nabla}^{\,2} \ + \ \mu^2 + \Pi(q, \rho(\vec{x}_2)) - E_\pi^2 \right] D_\pi^{FN}(\vec{x}_1, \vec{x}_2, E_\pi) = \\ \int \frac{d^3q}{(2\pi)^3} \frac{\omega(\vec{q})^2 - E_\pi^2}{E_\pi^2 - \omega(\vec{q})^2} \phi_\pi(\vec{q}, \vec{x}_1) \phi_\pi^*(\vec{q}, \vec{x}_2) = -\delta^3(\vec{x}_1 - \vec{x}_2) \ , \end{aligned} \tag{26}$$

where in the last step we use the fact that the pionic wave functions form a complete set of states.

We can proceed equally with the nuclear matter propagator and we obtain

$$\left[-\vec{\nabla}^{\,2} \quad + \quad \mu^2 + \Pi(q,\rho(\vec{x}_2)) - E_\pi^2\right] D_\pi^{NM}(\vec{x}_1,\vec{x}_2,E_\pi) = \int \frac{d^3q}{(2\pi)^3} \frac{\vec{q}^{\,2} + \mu^2 + \Pi(q,\rho(\vec{x}_2)) - E_\pi^2}{E_\pi^2 - \vec{q}^{\,2} - \mu^2 - \Pi(q,\rho(\vec{x}_2))} \mathrm{e}^{i\vec{q}(\vec{x}_1-\vec{x}_2)} = -\delta^3(\vec{x}_1-\vec{x}_2) \ . \quad (27)$$

The integral over $\vec{q}$ gives the same results in eqs. (26) and (27), leading to a local function, and providing further insight in the meaning of the LDA approximation in inclusive processes.

Note also that for a fixed E_π of the pion, the value of q at the pole of the two propagators is different, but also its meaning. In the case of finite nuclei we have $E_\pi = \omega(\vec{q})$ and the value of $\vec{q}$ is the asymptotic one when the pion leaves the nucleus. In the case of infinite nuclear matter we have $E_\pi^2 = \omega(\vec{q})^2 + \Pi(E_\pi, q, \rho(\vec{r}))$ which gives

$$E_\pi \simeq \omega(\vec{q}) + \frac{\Pi(r)}{2\omega(\vec{q})} \equiv \omega(\vec{q}) + V_{opt}(r) \ . \quad (28)$$

Hence, in this latter case, the value of q is the local momentum of the pion such that the total energy, kinetic plus potential, is the asymptotic energy of the pion.

2.2 The mesonic width and the occupation number

We have seen that Pauli blocking is the major factor in reducing the mesonic width of heavy Λ hypernuclei. It was suggested that because real interacting nuclei have the "occupied" states partly unoccupied, the mesonic width should be enhanced with respect to a calculation with fully occupied states up to the Fermi level [19]. In the nuclear matter approach of Sect. 2.1.1 this is easily visualized by recalling a realistic picture of the occupation number of the Fermi sea [20], which is depicted in fig. 5. For the states below the Fermi momentum the level of occupancy is of the order of 85% and, by assuming that in the Λ decay the nucleons can occupy the 15% vacancy of these states, we would guess that the mesonic width would stabilize at the level of about 10% of the free width for heavy nuclei (taking into account the absorption of pions on their way out of the nucleus). If this were the case the mesonic width could serve as a measure of the occupation number in the Fermi sea. The argument is very appealing and intuitive, however, it is incorrect and leads to an overestimate of the width by about three orders of magnitude in heavy nuclei.

The detailed discussion of this problem was done in ref. [21]. The falacy in the argumentation lies in the the following: since the Fermi distribution $n(\vec{p})$ of eq. (6) is only a first approximation to the momentum distribution, it looks like a sensible improvement to substitute the nucleon Fermi propagator of eq. (6) by

$$\frac{1-n_1(\vec{k})}{k^0 - E(\vec{k}) + i\epsilon} + \frac{n_1(\vec{k})}{k^0 - E(\vec{k}) - i\epsilon} \ , \quad (29)$$

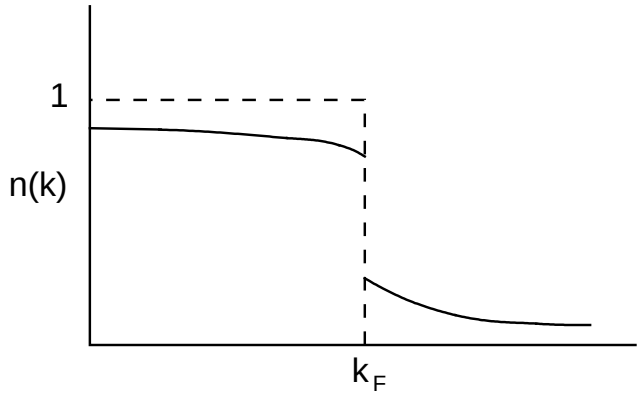

Figure 5: Schematic representation of the nucleon occupation number for an interacting Fermi sea.

where $n_1(\vec{k})$ is the realistic occupation number in nuclear matter and is then $\neq 0$ for all values of $\vec{k}$. This is actually and approximation often found in the literature, particularly in works of condensed matter and heavy ions. Given the analytical structure of the propagator, eq. (29), identical to the one of eq. (6), the formal result for the width is the same as in eq. (10) replacing only $1 - n(\vec{k} - \vec{q})$ by $1 - n_1(\vec{k} - \vec{q})$, in which case we would find widths of the order of 15% of the free width. However, eq. (29) is not an improvement over the propagator of eq. (6), but quite the opposite, as we shall see. The realistic nucleon propagator for an interacting Fermi sea is given in terms of the spectral functions by

$$G(k^0, k) = \int_{-\infty}^{\mu_p} d\omega \frac{S_h(\omega, k)}{k^0 - \omega - i\epsilon} + \int_{\mu_p}^{\infty} d\omega \frac{S_p(\omega, k)}{k^0 - \omega + i\epsilon} \ , \tag{30}$$

with μ_p the chemical potential.

When performing the calculations of the mesonic width with this nucleon propagator one obtains the factor

$$\int_{\mu_p}^{\infty} d\omega S_p(\omega, \vec{k} - \vec{q}) 2\pi\delta(k^0 - \omega - \omega(\vec{q})) \tag{31}$$

replacing the factor

$$[1 - n(\vec{k} - \vec{q})] 2\pi\delta(k^0 - E(\vec{k} - \vec{q}) - \omega(\vec{q})) \tag{32}$$

in eq. (5), when the Pauli blocking factor of eq. (10) is implemented. Eqs. (31) and (32) bare some intuitive resemblance because

$$\int_{\mu_p}^{\infty} d\omega S_p(\omega, \vec{k} - \vec{q}) = 1 - \int_{-\infty}^{\mu_p} S_h(\omega, \vec{k} - \vec{q}) d\omega = 1 - n_1(\vec{k} - \vec{q}) \ . \tag{33}$$

However, the presence of the δ function in eq. (31) prevents from factoring out the integral of S_p shown in eq. (33). Furthermore, because of restrictions of the phase space (energy and momentum conservation) the range of values of ω allowed are very small compared to the range (μ_p, ∞) needed in eq. (33) to obtain $1 - n_1(\vec{k} - \vec{q})$ of the interacting Fermi sea. In physical terms we can interprete it in the following way: the occupation number $n_1(\vec{k} - \vec{q})$ is an integral for all the energies of the nucleon, ω, of the probability of finding a nucleon with momentum $\vec{k} - \vec{q}$ and an energy ω, which is given by the spectral function $S_h(\omega, \vec{k} - \vec{q})$. However, in a physical decay process we have conservation of energy and momentum and hence there are severe restrictions to the values of the energies that the nucleon can have. This is why the occupation number $n_1(\vec{k} - \vec{q})$ cannot be factored out.

The actual calculations carried out in ref. [21] showed that for light and medium nuclei the use of the spectral representation for the nucleon propagator, eq. (30), instead of the one of the noninteracting Fermi sea, eq. (6), has negligible consequences in the mesonic width (of the order of 6% corrections in ${}^{16}_{\Lambda}\mathrm{O}$). The corrections can be of the order of 50% in heavy nuclei, but in all cases, when the pionic renormalization is taken into account, one can disregard these effects.

These findings have been of relevance in showing similar problems in the study of other physical processes, like in the contribution of the pion cloud to K^+ nucleus scattering where it is shown [22] that one cannot relate the effect of the pion cloud to the pion excess number in the nucleus as assumed in refs. [23,24]. Similar spectacular differences between the use of the occupation number and the spectral function are seen in the study of the nuclear structure functions of deep inelastic scattering at values of $x > 1$ [25]. For values of $x = 1.3$ the use of the occupation number gives values of the structure function two orders of magnitude bigger than the results with the spectral functions, which agree with experiment [26].

2.3 Results for the mesonic width

We separate here three regions of heavy, medium and light nuclei, where different physical phenomena are explored by means of the mesonic decay.

Experimental data for light and medium nuclei of the last decade can be found in [27, 28, 29, 30, 31].

2.3.1 Medium and heavy nuclei

In refs. [15,16,17] one can find abundant results in different nuclei which are rather realistic. These results have been recently improved [32] by a more accurate description of the energy balance in the particular reactions, taking into account transitions to the bound and continuum nucleon states and using a pion nucleus optical potential which has been derived theoretically and leads to a good description of pionic atoms data and of elastic, reaction and absorption cross sections in the scattering processes [33]. The imaginary part of the pion nucleus optical potential is split into two terms related to pion absorption and quasielastic scattering. In [32] the pion quasielastic events are

not removed from the pion flux, as it corresponds to the actual experimental observation, while the use of a full distortion of the pion with the total optical potential, as done in [15,16,17], inevitably removes the pion quasielastic events, together with the pion absorption events. Though conceptually important, this refinement turns out to be of little practical relevance in the present problem given the small energy that the pions carry and the very small phase space for quasielastic collisions [32]. However, other considerations, particularly the energy balance in the reactions, makes the widths in heavy nuclei for π^--decay about one order of magnitude smaller than those of ref. [17].

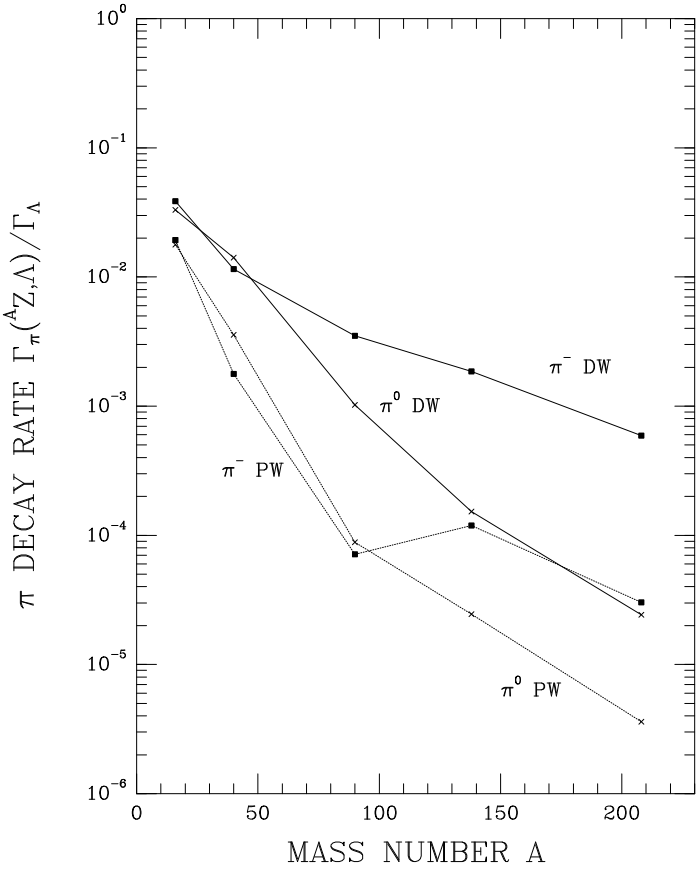

Figure 6: Pionic decay rate for π^0 and π^- as a function of the mass number (of the host nucleus, ^{16}O, ^{40}Ca, ^{90}Zr, ^{138}Ba, and ^{208}Pb). The two lower lines show the calculation with plane waves for the pion and the two upper lines the results with pion distorted waves.

In fig. 6 we show the prediction of ref. [32] for different nuclei and for π^0 and π^- decay, with plane waves and the renormalized pion wave function. The drastic effects of the pion renormalization are seen there and are a bit smaller than in former works because the energy balance forces the pions to come out with smaller energies than in the previous approaches and the attractive effects of the p-wave part of the optical potential are then diminished. Shell effects and energy balance are important here

because of the small energies left for the pions. They are responsible for the slight increase of the Λ width in ${}^{139}_{\Lambda}$Ba with respect to ${}^{91}_{\Lambda}$Zr seen in the figure for the plane wave calculation. When the interaction of the pions with the nucleus is considered, the extra attraction felt by the pions gives more room for pionic decay such that the nuclear energy differences in the energy balance are not so crucial.

2.3.2 Shell effects in medium nuclei

The energy balance for some nuclei makes the results somewhat surprising. Of particular relevance are the results in ${}^{12}_{\Lambda}$C shown in Table 1.

Table 1: Pionic partial decay rates in the decay of ${}^{12}_{\Lambda}$C

	$\Gamma_{\pi^0}/\Gamma_\Lambda$	$\Gamma_{\pi^-}/\Gamma_\Lambda$	$\Gamma_{\pi^0}/\Gamma_{\pi^-}$
[32]	0.159	0.086	1.86
[17]	0.13	0.098	1.32
EXP: [30]		$0.052^{+0.063}_{-0.035}$	
EXP: [31]	0.217 ± 0.084		

In ref. [16], using different pion optical potentials, the authors quote 0.169 and 0.126 for $\Gamma_{\pi^0}/\Gamma_\Lambda$ and 0.134 and 0.107 for $\Gamma_{\pi^-}/\Gamma_\Lambda$. Although with large errors, the experimental results confirm these striking theoretical predictions which show a large departure from the $\Delta I = 1/2$ rule in nuclei. Indeed, we would naively expect $\Gamma_{\pi^0}/\Gamma_{\pi^-} \sim 0.5$ (this should be the case for $N = Z$ core nuclei), while it is of the order of 2 for the results of ref. [32] and slightly larger than one for the results of refs. [16, 17]. This is mostly due to nuclear shell effects because of the large differences between the Q values met in these reactions.

2.3.3 Light nuclei: Short range repulsion and quark models

Another interesting finding is seen in very light nuclei. The mesonic width of ${}^{5}_{\Lambda}$He has attracted particular attention. There, in addition to the pion renormalization, the repulsive character of the ΛN interaction and the relatively weaker medium range attraction, compared to the NN interaction, push the Λ wave function to the surface of the nucleus, weakening the Pauli blocking effect and thus enhancing the mesonic decay [34, 35]. The experimental numbers clearly favour potentials with a repulsive ΛN core. One should note that such a repulsion automatically appears in quark based models of the ΛN interaction [36]. The study of the ${}^{5}_{\Lambda}$He decay using a quark model based hypernuclear wave function [37] leads to the results shown in Table 2, where they are compared to those of [38], which uses a Λ wave function from the modified YNG ΛN interaction [39] with a strong short range repulsion, and to those of [40] for the Isle Λ-nucleus repulsive potential at short distances [41].

There is a fair agreement of the theoretical results [37,38,40] with experiment [30], account taken of the large experimental errors.

Although the effect of the renormalization of the pion in the medium leads to an enhancement of the inclusive mesonic rate, it is possible to find particular decay

Table 2: Pionic partial decay rates in the decay of ${}^{5}_{\Lambda}$He

	$\Gamma_{\pi^-}/\Gamma_\Lambda$	$\Gamma_{\pi^0}/\Gamma_\Lambda$	$\Gamma_\pi/\Gamma_\Lambda$
[37]	0.431	0.239	0.670
[38]	0.393	0.215	0.547
[40]	0.40	0.20	0.5
EXP: [30]	0.44 ± 0.11	0.18 ± 0.20	$0.59^{+0.44}_{-0.31}$

channels where the effect is reversed. This has been shown in ref. [42] for the decay ${}^{4}_{\Lambda}\mathrm{H} \rightarrow {}^{4}\mathrm{He} + \pi^-$. The final nucleus ^{4}He selects the s-wave part of the pion optical potential, which is repulsive, hence leading to a reduction of the rate with respect to a calculation using free pion waves. This also means that, through the study of the mesonic decay in selected channels, one can learn about different parts of the pion nucleus optical potential.

The mesonic decay of the hypertriton, ${}^{3}_{\Lambda}$H, has also been studied recently [43], using wave functions for the hypertriton, $3N$ bound and $3N$ scattering states which are solutions of the Faddeev equations. The ^{3}He$+\pi^-$, $p+d+\pi^-$ and $p+p+n+\pi^-$ decay channels and the corresponding ones for π^0 have been studied. The total mesonic width is 92% of the free Λ width and compares favourably with the experimental data for the hypertriton lifetime, which ranges between $(2.20^{+1.02}_{-0.53}) \times 10^{-10}$ sec to $(2.64^{+0.92}_{-0.54}) \times 10^{-10}$ sec [44].

An interesting problem related with the decay of light hypernuclei is the ratio π^+/π^- in the decay of ${}^{4}_{\Lambda}$He. This ratio is measured to be about 5% and cannot come from the direct decay of the Λ ($\Lambda \rightarrow \pi^- p$, $\pi^0 n$). The problem concentrated some attention in the past [45], where rescattering of the π^0, $\pi^0 + p \rightarrow \pi^+ + n$, or Σ^+ decay, $\Sigma^+ \rightarrow \pi^+ n$, following the $\Lambda p \rightarrow \Sigma^+ n$ conversion were considered. However, the results gave a fraction much too small compared to experiment. The problem was revived recently [46], using updated information, and a result for that fraction of 1.2% was obtained, which, although being a factor of two larger than in [45], is still too small compared with the experimental value.

A more recent work [47] proposes a solution which consists of adding to the ${}^{4}_{\Lambda}$He wave function some $\Sigma^+ + {}^3$H component, which is relatively sizable in view of the strong $\Lambda N \rightarrow \Sigma N$ conversion. The Σ^+ would then decay into $\Sigma^+ N \rightarrow \pi^+ n N$, which leads to a s-wave spectrum as observed experimentally [48].

On the other hand, a different view is taken in [49], where it is suggested that the $\Delta I = 3/2$ component of the weak interaction is the responsible for the relatively high fraction of π^+ emission.

2.4 Conclusions on mesonic Λ decay

We have made a review of the present situation concerning the mesonic decay of Λ hypernuclei. We have established the formal link between the propagator method, where the huge enhancement of the pionic decay width was first reported, and the finite nuclei approach with wave functions and matrix elements. Shell effects and precise values of the nuclear binding energies are also important in the mesonic width

and they are best taken into account in the finite nuclei approach. The intuitive and appealing, but falacious, link between the nucleon occupation number and the mesonic width has also been discussed, which has served to unveil rough approximations used in other processes to link the pion excess number with contributions of the nuclear meson cloud to some physical observables, like K^+ nucleus scattering or deep inelastic scattering. We have also discussed the relevance of the short range ΛN repulsion in the mesonic width of light hypernuclei and showed how different models, all of them accounting for this repulsion, can provide a fair description of the experimental data. We should note in this respect that microscopical quark models lead naturally to such kind of repulsion, although a description in terms of the more conventional meson exchange picture is also posible.

With the limited amount of experimental data available on the mesonic channel, the amount of physical information obtained is remarkable. As just mentioned, there is support for strong ΛN repulsion at short distances. The process also provides us with the most striking renormalization effect due to the pion nucleus interaction. The sensitivity of the Λ decay to the pion nucleus optical potential can serve as a tool to choose between different theoretical descriptions of the complex mechanisms of pion nucleus interaction. The decay channel into π^0 can be an excellent instrument to learn about π^0 nucleus interaction, and so on.

It is clear that a systematic experimental search in many nuclei of the mesonic decay channel will provide us with very valuable information to unravel the intricancies of the pion nucleus interaction or the elementary properties of the ΛN interaction, as well as proper nuclear structure details of the Λ hypernuclei themselves.

3 Weak non-mesonic decay of Λ hypernuclei

The pionic decay mode of Λ hypernuclei is negligibly small in medium to heavy hypernuclei due to Pauli blocking acting on the final nucleon which emerges with a very small momentum. However, the medium effects are responsible for the opening of new decay channels, where there are no pions in the final state. These non-mesonic decay modes of Λ hypernuclei can be viewed as coming from the mesonic decay when the pion is produced in a virtual state and absorbed by one or more nucleons. The one-nucleon induced decay mode corresponds to the $\Lambda N \to NN$ transition and can be interpreted as being mediated by the exchange of one pion (or more massive mesons). In the two-nucleon induced decay of nuclei, the transition $\Lambda NN \to NNN$ can be interpreted as coming from the absorption of the virtual pion by a pair of nucleons that are correlated by the strong interaction. No matter what the interpretation of the different non-mesonic decay mechanisms is, what happens is that the mass excess in the initial state (176 MeV) is now converted exclusively into kinetic energy of the final nucleons, which may emerge with large momentum values not restricted by Pauli blocking. Hence, except for the very lightest ones, Λ hypernuclei decay mainly through the non-mesonic mechanisms.

3.1 One-nucleon induced decay

The decay of hypernuclei through the one-body induced mechanism $\Lambda N \to NN$ offers the best opportunity to study the $\Delta S = -1$ nonleptonic weak interaction between hadrons due to the practical impossibility of having stable Λ beams. Since the typical momentum exchanged is around 400 MeV/c, the process is short ranged and will not be too sensitive to the nuclear structure details. The $\Lambda N \to NN$ reaction, similar to the $\Delta S = 0$ $NN \to NN$ weak reaction but in the $\Delta S = -1$ sector, allows one to study not only the parity violating (PV) part of the interaction, but also the parity conserving (PC) one which, in the $NN \to NN$ case, is masked by the strong interaction. Note, however, that the study of the inverse reaction $pn \to p\Lambda$ with moderate energy and high intensity proton beams could be feasible at RCNP (Osaka) [50] or COSY (Jülich) [51].

The non-mesonic decay of hypernuclei has been studied for more than thirty years. The experimental and theoretical status on the one-nucleon induced hypernuclear decay was extensively reviewed by Cohen in 1990 [6]. For this reason we will just update the present situation in the next paragraph and only the new achievements made since 1990 and how they compare with previous works will be covered in more detail in the coming sections.

Block and Dalitz [52] built a phenomenological model to describe the decay of s-shell hypernuclei in terms of a few elementary spin-isospin reaction rates. Although no assumptions were made on the dynamics of the $\Lambda N \to NN$ reaction, this model has been (and is) extremely useful because, by fitting to the empirical data for light hypernuclei, one can extract information on the characteristics of the reaction, such as the validity of the $\Delta I = 1/2$ rule. The first microscopic calculation was that of Adams [53] who considered the one pion exchange mechanism to describe the non-

mesonic decay of a Λ in nuclear matter and found a large sensitivity to the short range correlations (SRC) induced by the strong interaction in the initial ΛN and final NN states. A unified treatment of the mesonic and non-mesonic channels based on Feynman diagrams and propagators was developed by Oset and Salcedo [13], where the medium effects in the renormalization of the pion were considered. Being a short range process, it was clear that the one pion exchange (OPE) mechanism might be insufficient to explain the data. McKellar and Gibson [54] made the first attempt to include the heavier mesons by developing a model for the exchange of the ρ meson. This was applied later to the decay of light hypernuclei [55] but the results depended on the relative sign between the π and ρ mechanisms that was not fixed by the model. Based on a pole model for the PC vertices and on soft meson theorem techniques for the PV ones, Dubach et al. [56] constructed a full one meson exchange potential and preliminary results for nuclear matter were obtained. The details of the model and final results have recently become available [57]. An extension of the model including form factors and some exchange diagrams related to the antisymmetrization of the final two-nucleon state has been recently applied to the decay of finite hypernuclei [58]. The exchange of σ and ρ mesons has also been considered within the image of correlated two pion exchange, where Δ and Σ are excited in the intermediate state [59, 60, 61, 62]. A description of the $\Lambda N \to NN$ decay in terms of quark degrees of freedom was first attempted in refs. [63], where a hybrid model that combined a quark Hamiltonian at short distances and OPE at long distances was employed. Oka and collaborators [64] combined a direct quark mechanism with a one pion exchange contribution for the description of light hypernuclei. A more realistic Λ wave function was used in a more recent work [65], where also the phase between the direct quark and the pion mechanisms was established. One kaon exchange amplitudes, which partially cancelled the pion ones, were also calculated in ref. [66] together with the quark contributions. All the models and results of the recent works will be extensively reviewed below.

3.1.1 OPE results

The OPE mechanism for the $\Lambda N \to NN$ transition displayed in fig. 7 involves a weak and a strong vertex.

As already shown in eq. (1), the weak Hamiltonian is parametrized in the form

$$\mathcal{H}^{\rm W}_{\Lambda {\rm N}\pi} = iG_F\mu^2\overline{\psi}_{\rm N}(A_\pi + B_\pi\gamma_5)\vec{\tau}\vec{\phi}_\pi\psi_\Lambda \begin{pmatrix}0\\1\end{pmatrix} \ , \tag{34}$$

which implements the $\Delta I = 1/2$ rule through the isospin spurion $\binom{0}{1}$. The consequences of breaking this rule in the non-mesonic decay of hypernuclei have been recently explored and will be presented in Sect. 3.1.4.

For the strong vertex the pseudoscalar coupling

$$\mathcal{H}^{\rm S}_{\rm NN\pi} = ig_{\rm NN\pi}\overline{\psi}_{\rm N}\gamma_5\vec{\tau}\vec{\phi}_\pi\psi_{\rm N} \ , \tag{35}$$

has usually been taken since most calculations are nonrelativistic and this vertex is

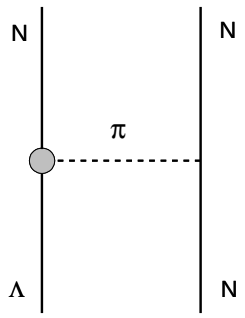

Figure 7: One pion exchange diagram for the $\Lambda N \to NN$ transition

equivalent to the pseudovector one. The nonrelativistic transition potential reads

$$V_\pi(\vec{q}) = -G_F \mu^2 \frac{g_{\rm NN\pi}}{2M} \left(A_\pi + \frac{B_\pi}{2\overline{M}} \vec{\sigma}_1 \vec{q} \right) \frac{\vec{\sigma}_2 \vec{q}}{\vec{q}^{\,2} + \mu^2} \vec{\tau}_1 \vec{\tau}_2 \tag{36}$$

where $\vec{q}$ is the momentum carried by the pion directed towards the strong vertex, μ the pion mass, M the nucleon mass and $\overline{M}$ the average between the nucleon and Λ masses.

By introducing the tensor operator $S_{12}(\hat{r}) = 3(\vec{\sigma}_1 \hat{q}\,)(\vec{\sigma}_2 \hat{q}\,) - \vec{\sigma}_1 \vec{\sigma}_2$, the OPE transition potential can be splitted into central, tensor (adding to a total PC part) and PV pieces. The decay rate can be obtained in terms of $< f \mid V_\pi \mid i >$, the expectation value of the potential between initial ΛN and final NN two-body states.

There are a few relativistic corrections which can be implemented. The vertices can be made relativistic (see eq. (32) of [67] and eq. (3) of [68]) and the pion propagator non-static, i.e., $\vec{q}^{\,2} \to -q^2$. Furthermore, one should use, for consistency, relativistic wave functions [69, 70]. Both types of corrections are of the order of 10% and of opposite sign, so we shall ignore the relativistic effects in what follows.

a) Nuclear matter

The first work to consider the OPE mechanism was that of Adams [53], where the importance of strong and final state interactions in the $\Lambda N \to NN$ transition was first pointed out. The calculation was made in nuclear matter and only the $L = 0$ ΛN relative motion was retained. The same approach was followed by McKellar and Gibson [54] who made the first attempt to improve on the OPE mechanism by including the ρ meson as well. This will be discussed in the next section. Their uncorrelated one-pion rate was consistent with that of Adams, after correcting the too small coupling constant, but the effect of correlations was found less strong. This was confirmed by the two other nuclear matter calculations that appeared at that time. Oset and Salcedo [13] used a Green's functions formalism to treat the mesonic and non-mesonic channels in a unified way. Their method includes automatically all the partial waves of the relative ΛN motion. The OPE mechanism was also studied

by Dubach and collaborators in the context of a one meson exchange model for the $\Lambda N \to NN$ transition [56, 57].

The results for the one-nucleon induced non-mesonic decay rate in nuclear matter are summarized in Table 3. The values of this table, and all others referring to decay rates, will be given in units of the free Λ width, $\Gamma_\Lambda = 3.80 \times 10^9$ s^{-1}. The uncorrelated results obtained by the various groups are very similar. Substantial diferences are found when SRC are considered, although Adams used an unusually strong tensor correlation that, when omitted, would bring the correlated result up to 1.57. The discrepancy of a factor of 2 between refs. [13] and [54], when form factors and short range effects tied to the initial and final strong correlations are included, can be understood from differences in the model ingredients. In ref. [54] a combined form factor of the type $\Phi(\vec{q}) = (\Lambda_\pi^2 - \mu^2)/(\Lambda_\pi^2 + \vec{q}^{\,2})$ is employed with $\Lambda_\pi^2 = 20\mu^2$, while ref. [13] uses this monopole form factor at each vertex with $\Lambda_\pi = 1300$ MeV. For the relevant momentum transfer of 400 MeV/c, the ratio of form factors squared is 1.8, while the different correlation functions account for the remaining difference. McKellar and Gibson use a Gaussian type, $1-\exp(-r^2/b^2)$, with $r = 0.75$, while Oset and Salcedo use a Bessel type, $1 - j_0(q_c r)$, with $q_c = 3.93$ fm^{-1}. As seen in ref. [71], the rates calculated with these two choices differ by about 30% and the Bessel type is closer to what is obtained from microscopic G-matrix calculations using the Nijmegen ΛN interactions.

Table 3: One pion exchange contribution to the Λ non-mesonic decay rate in nuclear matter.

Group	uncorr.	corr. (no FF)	corr. + FF
Adams [53]	3.47*	0.38	
McKellar-Gibson [54]	4.13	2.31	1.06
Oset-Salcedo [13]	4.3		2.2
Dubach et al. [57]	4.66	1.85	

* Corrected by a factor of 6.81 as pointed out in ref. [54]

In summary, the uncorrelated OPE contribution to the Λ decay rate in nuclear matter turns out to be around 4 times the free Λ width and the results are lowered by a factor of 2 when appropriate short range correlations in the initial and final state are considered.

b) Finite nuclei

The existence of new experimental data for the non-mesonic decay rates [30, 72] and the possibility of obtaining polarization observables, such as the asymmetry in the distribution of protons emerging from the weak decay of $^{12}_{\Lambda}$C [73] motivated a new calculation of the non-mesonic decay performed directly for the finite hypernuclear system [69, 70]. The formalism was chosen relativistic in view of the success of this model in reproducing polarization observables in proton nucleus scattering reactions.

The $\Lambda N \to NN$ transition was obtained from the relativistic Feynman amplitude

$$t_{fi} = iG_F\mu^2 g_{\rm NN\pi} \int d^4x d^4y \overline{\Psi}_{\vec{k}_1}(x)(A+B\gamma_5)\Psi_{\alpha_\Lambda}(x)\Delta_\pi(x-y)f(\mid \vec{x}-\vec{y}\mid)\overline{\Psi}_{\vec{k}_2}(y)\gamma_5\Psi_{\alpha_{\rm N}}(x)\,, \tag{37}$$

where the initial Λ and nucleon were solutions of the Dirac equation with scalar and vector potentials, chosen to reproduce the nucleus form factor and the nucleon and Λ separation energies. The two emerging nucleons felt the effect of a relativistic optical potential. The short range effects were considered via a phenomenological correlation function, f, modifying the pion propagator Δ_π. The value of the free rate for ${}^{12}_{\Lambda}$C was found to be about a factor of 2 smaller than the nuclear matter results. This is reasonable because a finite hypernucleus has low density regions which give a smaller contribution to the decay rate. It was surprising, however, that the rate was reduced by a factor of four due to SRC and FF at the vertices, an effect twice as large as that observed in the nuclear matter calculations. To adscribe the differences to the finite size of the system is not reasonable because correlations are short ranged and they should affect similarly the infinite and finite systems. Another possibility would be to relate the discrepacies to the relativistic model but ref. [69] already showed that, in the absence of correlations, the relativistic and nonrelativistic treatments were giving the same results to within 10%.

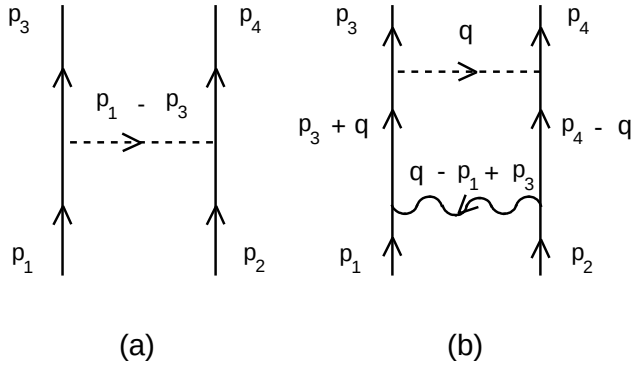

Figure 8: Schematic model for correlations in the OPE potential. Bare OPE diagram (a) and OPE with simultaneous exchange of a heavy meson (b).

The answer to this problem was partially given in ref. [74], where it was shown, through a nonrelativistic reduction of the correlated Feynman amplitude of eq. (37), that one did not obtain the same correlated potential as the one used in the nonrelativistic approaches, namely $f(r)V_\pi(\vec{r})$. The final answer was given in ref. [71] where, through a microscopic model for correlations, it was shown that the correct procedure is that followed by the nonrelativistic models. The essential point is that the origin of correlations is tied to the exchange of a heavy meson, as e.g. the ω meson, represented by the wavy line in fig. 8. Then the vertices involved in the weak transition mediated by the pion (dashed line) connect final state spinors with intermediate

spinors which depend on the momentum over which one must integrate. This can be clearly seen from the momentum space expression corresponding to the PC piece of the weak transition potential

$$\int \frac{d^3q}{(2\pi)^3} D(\vec{q}) \bar{u}(\vec{p}_3)\gamma_5 u(\vec{p}_3+\vec{q}) \bar{u}(\vec{p}_4)\gamma_5 u(\vec{p}_4-\vec{q}) \ldots \tag{38}$$

where $D(\vec{q})$ is the pion propagator and the dots simbolize additional elements of the amplitude which are not relevant for the discussion. However, the relativistic procedure followed in refs. [69,70] was equivalent to working with external momentum spinors which, therefore, factorize out of the integral

$$\bar{u}(\vec{p}_3)\gamma_5 u(\vec{p}_1) \bar{u}(\vec{p}_4)\gamma_5 u(\vec{p}_2) \int \frac{d^3q}{(2\pi)^3} D(\vec{q}) \ldots \tag{39}$$

In coordinate space, this procedure leads to oscillating potentials [71] which produce an artefactual reduction of the rates.

The calculated non-mesonic decay rates of several hypernuclei have been reported recently [58] in the framework of a nuclear shell-model and a nonrelativistic transition operator. Details on how the hypernuclear transition amplitude can be decomposed in terms of two-body amplitudes for nucleons in any shell can be found in [75]. The nucleons and the Λ are described with harmonic oscillator wave functions, SRC are included via a phenomenological correlation function inspired in G-matrix calculations with realistic ΛN interactions and final state interactions (FSI) are treated in terms of two-body NN scattering states obtained from realistic NN interactions. A phenomenological form factor is included at each vertex as well. The effect of the different ingredients is visualized in Table 4 for the decay rate of ${}^{12}_{\Lambda}$C, splitted into central, tensor (adding to a total PC rate) and PV contributions.

Table 4: OPE contribution to the non-mesonic decay rate of ${}^{12}_{\Lambda}$C from ref. [58]

	FREE	SRC	SRC+FF	SRC+FF+FSI	
				phenom.	Nijm93
Central rate	0.282	3.4×10^{-3}	1.3×10^{-2}	4.2×10^{-3}	3.3×10^{-3}
Tensor rate	0.858	0.781	0.637	0.685	0.566
PC	1.140	0.785	0.650	0.689	0.531
PV	0.542	0.447	0.389	0.421	0.353
Γ/Γ_Λ	1.682	1.232	1.038	1.110	0.885

The free central rate is reduced drastically by SRC, however, most of its contribution comes from the delta function which is completely eliminated by the correlation function, which is zero at the origin. The tensor rate is reduced by 10% by SRC and by 20–35% once FF and FSI are included. The PV rate represents 40% of the total rate, differing from previous nuclear matter results, which reported either negligible [54] or 15% [56] contribution to the rate. However, a simple estimate of the PV

contribution, relative to the PC one, for the most relevant momentum transfer (400 MeV/c) gives

$$\left(\frac{A_\pi}{\frac{B_\pi q}{2M}}\right)^2 = 0.57 \ ,$$

which yields a 35% fraction of the total for the PV rate. The last two columns reflect the importance of using a realistic NN wave function in the final state. A phenomenological NN correlation function of the type $1 - j_0(q_c r)$, with $q_c = 3.93$ fm^{-1}, gives a rate 25% larger than that obtained from a NN wavefunction based on the Nijmegen93 potential [76]. The NN interaction is relevant because it modulates the wave function at the short relative distances and prevents the contribution from the short part of the interaction. One may wonder about the interaction of the emitted nucleons with the mean potential of the nucleus. This can be taken into account by means of a complex optical potential, the real part of which is moderate and has practically no effect in the transition rate. The imaginary part would induce a loss of flux due, in the present case, to NN collisions. However, the net effect is a redistribution of the original NN emission strength into different multinucleon channels [77] without modifying the original decay rate, which is the magnitude in which we are interested.

One of the interest in doing finite nuclei calculations was to establish the role of relative $L \neq 0$ motion in the non-mesonic weak decay. It was especulated that the p-shell rate would be basically coming from relative ΛN motion in P wave, due to supression of S-wave by the corresponding $L = 1$ center-of-mass wave function which is zero at the most probable back-to-back kinematics. However, it was found [78] that, after integrating over all possible angular possibilities, 90% of the p-shell contribution comes from the relative ΛN $L = 0$ motion, which has been confirmed by the most elaborated model of ref. [58].

In Table 5 finite nuclei results from different works are compared. The results within brackets, if available, correspond to the calculation omitting SRC, FF and FSI, which will be referred to as the uncorrelated ones.

Table 5: OPE contribution to the non-mesonic decay rate of hypernuclei. Results within brackets correspond to the calculation omitting SRC, FF and FSI.

	$^{5}_{\Lambda}$He	$^{12}_{\Lambda}$C
Takeuchi et al. [55]	(0.52) 0.14	
Dubach et al. [57]	(0.6) 0.9	(3.4) 0.5
	(1.6)	2.0 [79]
Parreño et al. [58]	(0.98) 0.5	(1.68) 0.89
Oset-Salcedo [13]	1.15	1.45
EXP:	0.41 ± 0.14 [30]	1.14 ± 0.2 [30]
		0.89 ± 0.18 [72]

Compared to the other predictions, a quite low rate for $^{5}_{\Lambda}$He is found in ref. [55]. Part of it is due to the use of a more realistic Λ wave function pushed to the surface

by the effect of the repulsive Λ nucleus interaction in light hypernuclei. But most of the reduced rate comes from a much stronger effect of FF and SRC as they use the model of ref. [54] discussed in the nuclear matter section. The recent results of Dubach et al. [57] are somewhat confusing and the lack of computational details makes the comparison with other works difficult. However, some general points are worth mentioning. Their uncorrelated rate for ${}^{12}_{\Lambda}$C is a factor 2 larger than that of [58] and the correlated one a factor 2 smaller, so the effect of correlations is substantially larger than that found in their nuclear matter results. It is also surprising that their correlated rate for ${}^{5}_{\Lambda}$He is larger than the uncorrelated one and a factor of 2 larger than the ${}^{12}_{\Lambda}$C result. An explanation could lie in the possibility of some misprints. Their ${}^{12}_{\Lambda}$C rate quoted more than 10 years ago in some conference proceedings [79] turns out to be around 2. Moreover, the preprint of their most recent paper [57] quotes 1.6 for the uncorrelated ${}^{5}_{\Lambda}$He result. This two corrections would lead to more consistent results and would differ only in a factor of two from those of ref. [58]. We note that the model of ref. [57] does not contain form factors at the vertices, which would provide some additional reduction. The LDA results of ref. [13] appear to be a little bit too high when compared to the direct calculations on finite nuclei. However, we have checked that, when using the same Λ wave function as in ref. [58] (slightly more extended), a similar correlation function —controlled in [13] by the Landau g'_Λ parameter—, and neglecting the pion renormalization, the LDA result lowers down to 1.05, nicely agreeing with the value 1.038 quoted in Table 4 without FSI effects, which are absent in [13]. This consistency check reinforces the idea that the LDA is an excellent tool to study processes that are not too sensitive to nuclear structure details or low energy nuclear excitations as is the case of the non-mesonic weak decay of hypernuclei.

After this comparison, we can safely claim that, in general, the OPE mechanism predicts non-mesonic decay rates of finite nuclei in agreement with the experimental values.

However, the OPE model is unable to explain the ratio Γ_n/Γ_p between the neutron-induced rate ($\Lambda n \to nn$) and the proton-induced one ($\Lambda p \to np$). In Table 6 several predictions for this ratio are compared with the experimental results. While the data, with large error bars, seem to suggest a value of around 1 or larger (except for the very light hypernucleus ${}^{4}_{\Lambda}$He [80,81]), all models give values around 0.05–0.2. This is a well known characteristic of the OPE mechanism, which favors the tensor transitions over the central and parity violating ones. Since the ΛN pair is mainly moving in $L = 0$ states and the tensor operator induces ${}^3S_1(\Lambda N) \to {}^3D_1(NN)$ transitions, the antisymmetric final system will be predominantly in an isospin I=0 state, which only np pairs can achieve. Hence, the transition $\Lambda n \to nn$ is highly suppressed in the OPE model. These arguments have been more quantitatively stated in ref. [5], within the propagator method. In the limit of zero momentum for the Λ and small Fermi momentum for the nucleons, the ratio Γ_n/Γ_p is 1/14 when the antisymmetry of the final two nucleons is taken into account. The ratio becomes 1/5 when the antisymmetry is neglected, while the total width is changed only at the level of 20%.

This discrepancy motivated the search for new mechanisms driving the $\Lambda N \to NN$ decay, such as the inclusion of other mesons, correlated two pion exchange, quark

Table 6: OPE results for the ratio Γ_n/Γ_p

		π (uncorr.)	π (corr.)
Takeuchi et al. [55]	(${}^{5}_{\Lambda}$He)		0.06
Inoue et al. [64]	(${}^{5}_{\Lambda}$He)		0.12
	(${}^{4}_{\Lambda}$He)		0.08
Parreño et al. [58]	(${}^{12}_{\Lambda}$C)	0.18	0.10
	(${}^{5}_{\Lambda}$He)	0.12	0.07
Dubach et al. [57]	(nuc. matt.)	0.09	0.06
	(${}^{12}_{\Lambda}$C)	0.22	0.20
	(${}^{5}_{\Lambda}$He)	0.07	0.05
EXP		${}^{4}_{\Lambda}$He	0.06 ± 0.30 [80]
			0.25 ± 0.13 [81]
		${}^{5}_{\Lambda}$He	0.93 ± 0.5 [30]
		${}^{12}_{\Lambda}$C	$1.33^{+1.12}_{-0.81}$ [30]
			$1.87^{+0.91}_{-1.59}$ [72]
			0.70 ± 0.30 [82]
			0.52 ± 0.16 [82]

model calculations, incorporation of $\Delta I = 3/2$ amplitudes, etc, all of which will be described in coming sections.

3.1.2 Meson exchange model beyond OPE

The OPE mechanism is an excellent starting point to study the weak $\Lambda N \to NN$ decay due to the experimentally known weak vertex. However, this mechanism can at most describe the long range part of the transition potential, while it was soon realized [53] that the large momentum exchanged (400 MeV/c) would probe quite short distances and more massive mesons might contribute in the decay process.

a) The ρ meson

Including the ρ meson in the weak decay mechanism was fist attempted by McKellar and Gibson [54], where the weak vertex Hamiltonian was

$$\mathcal{H}^{\rm W}_{\Lambda{\rm N}\rho} = G_F\mu^2\,\overline{\psi}_{\rm N}\,\left(\alpha\gamma^\mu - \beta i\frac{\sigma^{\mu\nu}q_\nu}{2\overline{M}} + \varepsilon\gamma^\mu\gamma_5\right)\vec{\tau}\vec{\rho}_\mu\psi_\Lambda\,\begin{pmatrix}0\\1\end{pmatrix}\ , \tag{40}$$

where, contrary to the pion, the weak constants α, β and ε must be determined theoretically. Taking the usual strong $\Lambda N\rho$ vertex

$$\mathcal{H}^{\rm S}_{\rm NN\rho} = \overline{\psi}_{\rm N}\left(F_1\gamma^\mu + i\frac{F_2}{2M}\sigma^{\mu\nu}q_\nu\right)\vec{\tau}\vec{\rho}_\mu\psi_{\rm N}\ , \tag{41}$$

the nonrelativistic reduction of the ρ transition potential reads

$$\begin{aligned} V_\rho(\vec{q}) \;\; = \;\; & G_F\mu^2\left(F_1\alpha - \frac{(\alpha+\beta)(F_1+F_2)}{4M\overline{M}}(\vec{\sigma}_1\times\vec{q})(\vec{\sigma}_2\times\vec{q})\right. \\ & \left. + i\frac{\varepsilon(F_1+F_2)}{2M}(\vec{\sigma}_1\times\vec{\sigma}_2)\vec{q}\right)\frac{1}{\vec{q}^{\,2}+m_\rho^2}\ . \end{aligned} \tag{42}$$

Using $(\vec{\sigma}_1 \times \vec{q})(\vec{\sigma}_2 \times \vec{q}) = (\vec{\sigma}_1\vec{\sigma}_2)\,\vec{q}^{\,2} - (\vec{\sigma}_1\vec{q})(\vec{\sigma}_2\vec{q})$, and decomposing $(\vec{\sigma}_1\vec{q})(\vec{\sigma}_2\vec{q})$ into central and tensor operators, this potential contains, as in the case of pion exchange, central, tensor and parity violating pieces.

Two weak coupling models are used in ref. [54], namely, a modified factorization approximation —omitting the factor $\sin\theta_c \cos\theta_c$— and a pole model which applies only to the PC amplitudes. The resulting coupling constants differ substantially in both approaches, the pole model giving a combination $(\alpha + \beta)$ which differs in sign and is a factor of 20 smaller than that obtained in the factorization approximation. Combining the OPE results with the ρ contribution with an arbitrary relative sign, gives, for the factorization approach, a non-mesonic rate which ranges between 0.7 (for $\pi - \rho$) and 2.3 (for $\pi + \rho$). Aware of the limitations of the factorization model, the authors of ref. [54] state that their estimates can vary up to a factor 3. An important observation was that, similarly as for their OPE results, only the tensor transition gave a non-negligible contribution to the ρ exchange weak amplitude.

Despite the large uncertainty in the result, an application of this model to finite nuclei was performed in ref. [55], where the decay rate of helium hypernuclei was explored. The $(\pi + \rho)$ model gave an amplification of their π-only result and the $(\pi - \rho)$ one lead to a complete cancellation. Although the ${}^{5}_{\Lambda}$He result was in nice agreement with the data in the $(\pi + \rho)$ model, the ${}^{4}_{\Lambda}$He rate was overestimated by a factor of 2.

Nardulli [83] obtains the weak ρ couplings via a pole model, including, in addition to the ground state baryon octet, the first excited $1/2^+$ baryons. However, it must be recalled [84] that their value for the $K \to \pi$ transition is an order of magnitude larger than what is obtained from the kaon decay mode $K \to \pi\pi$ [85]. The PV couplings were also calculated within a pole model including the negative parity $1/2^-$ baryon poles. By rescaling the results of ref. [54] according to the new coupling constants, Nardulli predicts the non-mesonic decay rate of a Λ in nuclear matter to be 0.7.

The ρ meson was also investigated in ref. [57] as a part of their full one meson exchange potential, which will be discussed in more detail below. Only the ground state baryons are considered in their determination of the PC coupling constants, while the PV ones are obtained applying soft meson theorems and current algebra techniques. Although the baryon pole diagrams could, in principle, also contribute to the PV couplings, they were estimated to be only a several percent of the leading current algebra contribution [85]. The contribution of the ρ meson, acting mainly on the $S \to D$ transition, was found to decrease the pion-only rate by 15%.

A thorough study of the ρ-meson contribution to the decay rate of ${}^{12}_{\Lambda}$C was performed recently [86], using the model of ref. [57] for the weak $\Lambda N\rho$ couplings and employing strong couplings from realistic YN potentials [87, 88]. One of the findings of that work is that the central amplitude of the ρ-meson contribution cannot be neglected and is, in fact, larger than the tensor one. The reason is that the function $j_2(kr)$, representing the outgoing relative NN wavefuntion, eliminates strength of the tensor potential from the short distances. Due to its shorter range, the tensor contribution of the ρ is strongly reduced with respect to the central transitions, which are governed by the function $j_0(kr)$. As can be seen in Table 7 the central rate for the ρ contribution turns out to be 3.5 times the tensor one, once one includes SRC,

FF and FSI (considered in a simplified way through the NN correlation function $f(r) = 1 - j_0(q_c r)$, with $q_c = 3.93$ fm^{-1}). The table shows that the ρ-meson reduces the π-only rate by 10%, similar to the 15% reduction reported in ref. [56], although a large fraction of the ρ-rate came from $S \to D$ transitions in the latter case. Similar qualitative conclusions are obtained when more realistic NN wavefunctions, based on a T-matrix calculation employing the Nijmegen93 potential [76], are used [58]. There, the central to tensor relative strength of the ρ meson is 1.5 and it reduces the π-only rate by 3%.

Table 7: The ρ, π and $\pi + \rho$ contributions to the decay rate of $^{12}_{\Lambda}$C from ref. [86].

	ρ		π	$\pi + \rho$
	uncorr.	corr.		
Central	0.658	0.085	0.004	0.059
Tensor	0.155	0.024	0.685	0.454
PV	0.109	0.011	0.421	0.477
Total	0.921	0.119	1.110	0.991

It is clear that other conclusions could be reached had one used a different model for the $\Lambda N\rho$ vertex. However, since the central and tensor potentials are weighted by the same $(\alpha + \beta)$ combination, it is quite likely that both central and tensor amplitudes are important and need to be included before any further improvement on the potential is made.

b) The full one meson exchange potential

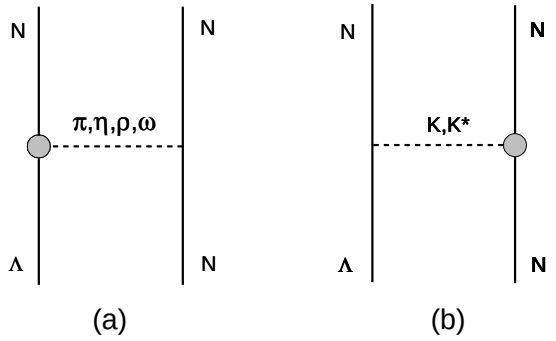

Figure 9: Non-strange (a) and strange (b) meson exchange contribution to the $\Lambda N \to NN$ weak transition potential. The weak vertex is indicated by the circle.

A one meson exchange model to describe the $\Lambda N \to NN$ transition was first reported in ref. [56] more than 10 years ago, and the details have recently become available [57]. As shown in fig. 9, pseudoscalar (π, η, K) and vector (ρ, ω, K^*) meson exchanges were included and the $\Delta I = 1/2$ rule at the weak vertex was assumed. The

PC part of the vertices was obtained from a pole model including both baryon and meson pole diagrams shown, respectively, in figs. 10 and 11, where the cross indicates a weak baryon→baryon or meson→meson weak transition. Employing $SU(6)_w$ symmetry and assuming PCAC, current algebra methods allow one to relate the baryon→baryon amplitudes to the experimentally known Λ and Σ decay p-wave amplitudes, and the meson→meson ones to the $K \to \pi$ one, which is determined from the physical $K \to \pi\pi$ decay rate. The strong couplings for the pseudoscalar mesons are obtained from SU(3) symmetry and the Goldberger-Treiman relation, while those of the vector mesons require the vector dominance assumption.

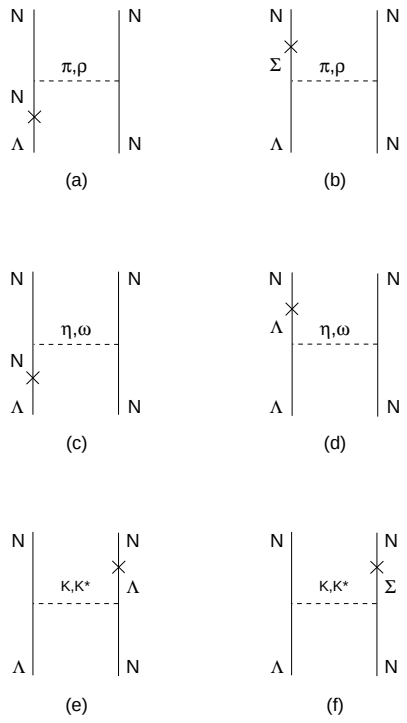

Figure 10: Baryon pole diagrams contributing to the PC weak vertices in the $\Lambda N \to NN$ transition amplitude.

This model was applied to obtain the non-mesonic decay rate of a Λ in nuclear matter [56, 57] and, later, predictions were also given for ${}^{5}_{\Lambda}$He and ${}^{12}_{\Lambda}$C [57], although no details are yet available.

Following the lines of refs. [56,57], a full one meson exchange potential has recently been constructed to study the non-mesonic decay rate of finite nuclei [58], where the nuclear structure details of the hypernucleus under consideration are carefully taken into account. A convenient compact expression for the potential is given by

$$V(\vec{r}) = \sum_i \sum_\alpha V_\alpha^{(i)}(\vec{r}) = \sum_i \sum_\alpha V_\alpha^{(i)}(r) \hat{O}_\alpha \hat{I}_\alpha^{(i)} \tag{43}$$

where the index i runs over the different mesons $(\pi, \eta, K, \rho, \omega, K^*)$ and α over the spin operators $\hat{O}_\alpha \in \{\hat{1}$ (Central spin independent), $\vec{\sigma}_1\vec{\sigma}_2$ (Central spin dependent), S_{12}

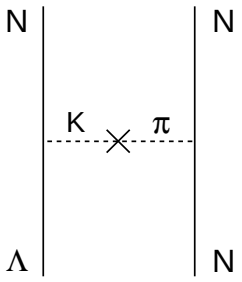

Figure 11: Meson pole diagram contributing to the $\Lambda N \to NN$ transition amplitude.

(Tensor), $\vec{\sigma}_2\hat{r}$ (PV for pseudoscalar mesons) and $(\vec{\sigma}_1 \times \vec{\sigma}_2)\hat{r}$ (PV for vector mesons)$\}$. The isospin operator $\hat{I}_\alpha^{(i)}$ is $\hat{1}$ for isoscalar mesons (η, ω), $\vec{\tau}_1\vec{\tau}_2$ for isovector mesons (π, ρ) and a combination of $\hat{1}$ and $\vec{\tau}_1\vec{\tau}_2$ for isodoublet mesons (K, K^*).

The detailed form of the potential and the explicit values of the coupling constants can be found in refs. [58, 75]. To facilitate the comparison, it is worth pointing out the differences with respect to the model of ref. [57]. In the first place, the strong coupling constants employed in ref. [58] are taken from realistic YN interactions, such as the Nijmegen [87] or the Jülich [88] ones. Secondly, the potential of ref. [57] does not contain form factors in spite of the large momentum transferred in the process which makes the pion to be far off-shell. Thirdly, a stronger correlation function is used in ref. [57], which in part can compensate for the lack of form factors. The work of ref. [58] uses a parametrization [74] which lies in between realistic correlation functions obtained from G-matrix calculations employing the Nijmegen soft- and hard-core potentials. Finally, the contribution of the meson pole diagrams to the PC couplings were found to be small and, hence, they were omitted in ref. [58].

Results obtained from both models are shown in Table 8, were the Λ decay rate in nuclear matter of ref. [57] is compared to that in ${}^{12}_{\Lambda}$C of ref. [58] for a sequential (and arbitrary) addition of the different mesons. Although the reduction with respect to the pion-only rate is similar when all the mesons are included (25% in the case of ref. [57] and 18% in the case of ref. [58]), a stronger sensitivity to the strange mesons is found in ref. [58].

The work of ref. [58] includes the mesons by isospin pairs $[(\pi, \rho)$, (K, K^*), $(\eta, \omega)]$ and finds important destructive interference effects for each isospin-like pair in the tensor transitions, which provide the most important contribution for pseudoscalar mesons. On the contrary, the PV rates tend to interfere constructively. The study also demonstrates the effect of including realistic NN scattering wave functions in the final state, reducing the pion-only rate of Table 7 from 1.11 to 0.89. The final results of ref. [58] for the non-mesonic decay rate of ${}^{12}_{\Lambda}$C are shown in Table 9, using the Nijmegen (Jülich) strong coupling constants. The ordering of the mesons is different from the previous table and reflects the isospin-pair study mentioned above. Table 9

Table 8: One meson exchange results for the non-mesonic decay rate.

Meson	ref. [57] (nuc. matt.)	ref. [58] $^{12}_{\Lambda}$C
π	1.85	1.11
$+\eta$	1.68	1.06
$+K$	1.31	0.54
$+\rho$	1.11	0.51
$+\omega$	1.19	0.58
$+K^*$	1.38	0.91

shows the significance of SRC,FF and FSI in the decay rate, drastically reducing the influence of the heavier mesons on the rate. The K meson lowers the rate by almost 50%, reduction that is partly compensated by its isospin partner, the K^*. The final result is either 15% smaller (using the Nijmegen couplings) or 15% larger (using the Jülich couplings) than the pion-only result. This sensitivity to the strong couplings is unfortunate since one expected to use the non-mesonic decay of hypernuclei to learn about the weak vertex. More data on YN scattering is highly desirable in order to reduce the uncertainties on the strong coupling constants. The table also shows the results when new K-meson weak couplings including one-loop corrections to the leading order in Chiral Perturbation Theory [89] are employed. Since the one-loop corrections decrease the tree-level p-wave amplitudes by 30%, the influence of the K-meson is reduced substantially giving rise to an increased rate. Note, however, that the effect of counterterms was ignored in ref. [89] and further investigations are necessary. In any case, any theoretical improvement in the determination of the weak and strong vertices can be easily incorporated in the meson exchange model of ref. [58].

Table 9: One meson exchange results for the non-mesonic rate of $^{12}_{\Lambda}$C, obtained in [58] using the Nijmegen (Jülich) strong couplings

Meson	uncorr.	corr.
π	1.68 (1.68)	0.89 (0.89)
$+\rho$	2.06 (2.33)	0.86 (0.83)
$+K$	1.34 (1.70)	0.50 (0.51)
$+K^*$	2.84 (3.82)	0.76 (0.90)
$+\eta$	2.47 (3.82)	0.68 (0.90)
$+\omega$	2.30 (4.34)	0.75 (1.02)
K-couplings from χPT		0.84 (1.10)

The available results for the non-mesonic weak decay of finite nuclei in the one meson exchange model are displayed in Table 10. The results for $^{12}_{\Lambda}$C of ref. [57] are extremely small when compared with their previous nuclear matter results shown in Table 8. They are a factor 7 smaller, which seems unreasonable since one may expect

reduction factors of at most 1.5 by going from nuclear matter to a finite nucleus as ${}^{12}_{\Lambda}$C. However, the results of the same group quoted in ref. [79], shown between brackets in Table 10, seem to be more consistent with their previous nuclear matter results, with the calculations of ref. [58] and with the experimental data. Taking these considerations into account we can say that, in general, the non-mesonic rates of finite hypernuclei obtained within the one meson exchange model are in fair agreement with the measured values.

Table 10: Non-mesonic decay rates within the meson exchange model of refs. [57] and [58].

	${}^{5}_{\Lambda}$He		${}^{12}_{\Lambda}$C	
	π	all mesons	π	all mesons
ref. [57]	0.9	0.5	0.5 (2.0 [79])	0.2 (1.2 [79])
ref. [58]	0.5	0.41	0.89	0.75
EXP:	0.41 ± 0.14 [30]		1.14 ± 0.2 [30]	
			0.89 ± 0.18 [72]	

The one meson exchange model has been recently applied to study the non-mesonic decay of the hypertriton, ${}^{3}_{\Lambda}$H [90]. The wave function of the hypertriton, obtained by solving the Fadeev equations based on realistic NN forces and the Nijmegen soft-core YN interaction, was found to reproduce nicely the Λ separation energy, $B_\Lambda = 0.13 \pm 0.05$ MeV [91]. The two non-mesonic decay modes, ${}^{3}_{\Lambda}\mathrm{H} \to d + n$ and ${}^{3}_{\Lambda}\mathrm{H}$ $\to nnp$, were investigated and the results are shown in Table 11. The one-pion only result turns out to be 1.7% of the free Λ decay rate, which is almost a factor 3 smaller than what was obtained in a simpler calculation [92], which ignored FSI. Indeed, the results in the table show that FSI have a strong influence on the rate, reducing the PWIA value by a factor of 2. Including all mesons decreases the one-pion result by around 10%. That work also makes extensive investigation of the kinematical regions where protons and neutrons coming from the partial neutron- and proton-induced mechanisms could be found. It was shown that the regions covered by the two mechanisms largely overlap and, therefore, the partial rates cannot be measured separately unless one applies kinematical detection constraints, which would then lead to the measurement of only fractions of these partial rates.

Table 11: Non-mesonic decay rate of ${}^{3}_{\Lambda}$H from [90]

	π	all mesons
$\Gamma^{n+d}_{\mathrm{PWIA}}$	0.0047	0.0037
Γ^{n+d}	0.0012	0.0017
$\Gamma^{n+n+p}_{\mathrm{PWIA}}$	0.036	0.028
Γ^{n+n+p}	0.018	0.015
Γ^{tot}	0.019	0.017

The construction of a meson exchange model was partly motivated by the unability of the OPE mechanism to explain the experimentally large neutron to proton ratio.

A summary of results for Γ_n/Γ_p is shown in Table 12. The spectacular increase in this ratio, especially for ${}^{12}_{\Lambda}$C, obtained in ref. [57] when all the mesons are included is not confirmed by the results of ref. [58]. It could be that the use of form factors, considered in ref. [58] and neglected in ref. [57], diminish the effect of the heavier mesons, due to the removal of strength at high momentum values and thus at short distances, which would then produce a ratio Γ_n/Γ_p largely dominated by the OPE value. In any case, the difference between the nuclear matter and ${}^{12}_{\Lambda}$C results in ref. [57] is somewhat surprising in view of the fact that we are dealing with a ratio of rates for which the short distances play the most relevant role. Details on the finite nucleus calculation of ref. [57] are awaited in order to clarify the origin of such differences.

Table 12: Neutron- to proton-induced ratio Γ_n/Γ_p.

		π	π, ρ	all mesons
	nuc. matter	0.06	0.08	0.34
ref. [57]	${}^{5}_{\Lambda}$He	0.05		0.48
	${}^{12}_{\Lambda}$C	0.20		0.83
ref. [58]	${}^{5}_{\Lambda}$He			0.07
	${}^{12}_{\Lambda}$C	0.104	0.095	0.07
EXP:				
[30]	${}^{5}_{\Lambda}$He	0.93 ± 0.5		
	${}^{12}_{\Lambda}$C	$1.33^{+1.12}_{-0.81}$		
[72]	${}^{12}_{\Lambda}$C	$1.87^{+0.91}_{-1.59}$		
[82]	${}^{12}_{\Lambda}$C	0.70 ± 0.30		
		0.52 ± 0.16		

The experimental values for Γ_n/Γ_p have large uncertainties due, mainly, to the difficulties in detecting neutrons. Less uncertain are the results for the proton-induced partial rate Γ_p and the available data are compared in Table 13 with the theoretical predictions of the meson exchange model of ref. [58].

Table 13: Proton-induced ratio Γ_p.

	EXP	ref. [58]	
		π-only	all mesons
${}^{4}_{\Lambda}$He	0.16 ± 0.02 [81]		
${}^{5}_{\Lambda}$He	0.21 ± 0.07 [30]	0.43	0.38
${}^{11}_{\Lambda}$B	$0.30^{+0.15}_{-0.11}$ [30]	0.64	0.56
${}^{12}_{\Lambda}$C	$0.31^{+0.18}_{-0.11}$ [30]	0.80	0.71

Obviously, the fact that the non-mesonic rate is well reproduced by this model while the ratio Γ_n/Γ_p turns out to be too small, leads necessarily to an overestimation (of almost a factor of 2) for Γ_p. It is somewhat surprising that, while both neutron- and proton-induced partial rates appear to be in disagreement with the data, their sum conspires to give a non-mesonic rate which reproduces the measurements. Although a

more proper comparison should be made after the experimental cut offs in the energy of the detected particles are implemented in the theoretical models, it is important to stress that precise measurements of Γ_p, more feasible experimentally than the ratio Γ_n/Γ_p, would bring valuable information to better understand the mechanism inducing the $\Lambda N \to NN$ transition.

c) Two pion exchange

The two pion exchange mechanism of fig. 12(a), containing a strong $\Lambda N \to \Sigma N$ transition plus a weak $\Sigma N \to NN$ one, was studied by Bandō et al. [93] together with the usual one pion mechanism for $\Lambda N \to NN$. The empirical $\Lambda N\pi$ and $\Sigma N\pi$ weak vertices were used and the $\Delta I = 1/2$ rule enforced. A closure approximation was employed to deal with the sum over intermediate states. The potential for the $\Lambda N \to \Sigma N \to NN$ transition was obtained for several partial waves and compared with the OPE ones. Important interference effecs for the final $I = 0$ channels (only accessible to $\Lambda p \to np$), constructive for ${}^3S_1 \to {}^3S_1$ and ${}^3S_1 \to {}^1P_1$ and destructive for ${}^3S_1 \to {}^3D_1$, were found. As a result the calculated proton-induced rate, Γ_p, for ${}^5_\Lambda$He is larger than the OPE value in about a factor 1.5. Moreover, the destructive interference in the $I = 1$ ${}^3S_1 \to {}^3P_1$ channel produces an overall decrease in the neutron-induced rate, Γ_n. Therefore, the $\Lambda - \Sigma$ coupling reduces the ratio Γ_n/Γ_p even more, from the OPE value 0.13 to 0.04.

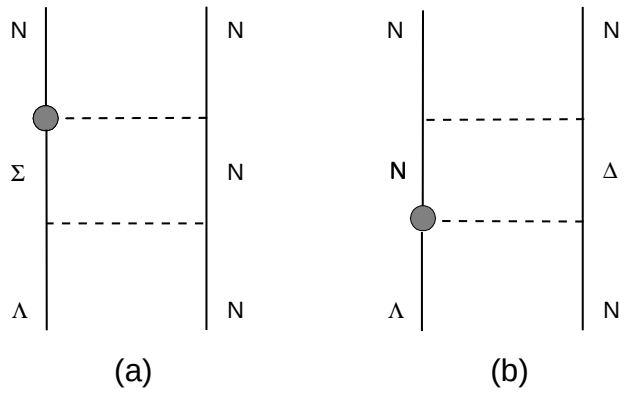

Figure 12: Two pion exchange amplitudes to the $\Lambda N \to NN$ transition through coupling to intermediate ΣN (a) or ΔN (b) states.

In ref. [59], this $\Lambda - \Sigma$ process was considered together with the mechanism $\Lambda N \to N\Delta \to NN$ of fig. 12(b). The loop in figs. 12 was computed explicitly and initial ΛN and final NN wavefunctions, correlated by the effect of the strong interaction, were used. Note that a potential source of doublecounting in the $\Lambda - \Sigma$ diagram may arise because realistic ΛN correlated wave functions have the $\Lambda N \to \Sigma N$ transition built inside. The results for the $\Lambda - \Sigma$ diagram are qualitatively different than those of ref. [93] since a reduction of 30% is found in both the ${}^3S_1 \to {}^3S_1$ and ${}^3S_1 \to {}^3D_1$

amplitudes. The $\Delta - N\ ^1S_0 \rightarrow ^1\ S_0$ amplitude is about a factor 1.5 larger than the OPE one and would give rise to an increase on Γ_n, although no rates, only amplitudes, were calculated in ref. [59].

In analogy with recent developments in the NN potential, in which the ρ and σ mesons are considered in terms of the exchange of two correlated pions, there have been recent attemps to incorporate this picture in the weak $\Lambda N \rightarrow NN$ transition potential [60, 61]. The $\pi\pi$ correlation is approximated, as displayed in fig. 13, by a t-channel resonance which can be either the scalar σ meson or the vector ρ meson. The weak vertex is obtained in both cases by means of a loop diagram with two pions and an intermediate N or Σ baryon. The strong vertex is generated in the same way in ref. [60], while phenomenological σNN and ρNN couplings from ordinary one meson exchange potentials that fit the NN scattering data are considered in ref. [61]. Note that the strength of the 2π contribution obviously depends on the cut off used to regularize the integrals in the triangle loops.

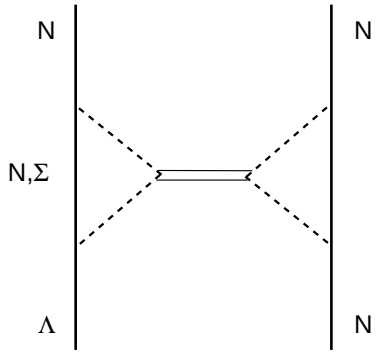

Figure 13: Correlated two pion exchange $\Lambda N \rightarrow NN$ transition, where the pions couple to σ or ρ mesons.

In ref. [60] a substantial contribution of the 2π diagram to the $^1S_0 \rightarrow ^1\ S_0$ amplitude, about 4 times larger than the OPE one, is found. For the other channels, the 2π contribution represents at most 30% of the π-only value. This is in contrast to what is found in ref. [61], where the $2\pi/\rho$ potential in the $^3S_1 \rightarrow ^3\ D_1$ channel tends to cancel quite strongly the π-only contribution. The $^1S_0 \rightarrow ^1\ S_0$ transition is also quite affected by the $2\pi/\rho$ and $2\pi/\sigma$ contributions, which have opposite sign than that for the π-only one, but not at the level of the factor 4 found in ref. [60].

The model of ref. [61] is applied to compute the partial non-mesonic decay rates of ${}^{12}_{\Lambda}$C [62]. It is found that the $2\pi/\rho$ amplitudes decrease the non-mesonic rate from 0.86 to 0.79 and including also the $2\pi/\sigma$ ones gives a final value of 0.92. The ratio Γ_n/Γ_p goes from the value 0.087 (π only) to 0.10 ($\pi + 2\pi/\rho$) and to a final 0.14 ($\pi + 2\pi/\rho + 2\pi/\sigma$), still far away from the empirical results.

3.1.3 Quark model based results

In recent works [64, 66] an old idea of treating the $\Lambda N \to NN$ mechanism from the point of view of quark degrees of freedom [63] is reexamined. In the latter reference a hybrid quark-hadron model was used in which the usual OPE between hadrons was adopted for the external region of relative ΛN distances ($r > r_0$ with $r_0 \simeq 0.8$ fm), while a six-quark wave function and an effective quark Hamiltonian is taken for $r_0 < 0.8$ fm. The main uncertainty within that model is the parametrization of the weak effective $\Delta S = 1$ quark Hamiltonian. Only when the coefficients of the QCD corrected Gilman and Wise Hamiltonian [94] are modified to implement the $\Delta I = 1/2$ rule, did the non-mesonic decay of ${}^{12}_{\Lambda}$C fall within the uncertainties of the experimental Brookhaven value of 1.14 ± 0.2 [30].

In refs. [64, 66] a four-quark $\Delta S = 1$ effective Hamiltonian, containing both $\Delta I = 1/2$ and $3/2$ terms and modified by QCD effects [95] was used, along with the quark cluster model for the quark component of the two-baryon initial and final states. Since quark-antiquark pairs are not allowed as intermediate states, the authors incorporate explicitly meson exchange diagrams, as the π meson [64] and also the K meson [66].

Both works find large $\Delta I = 3/2$ contributions to the ${}^1S_0 \to {}^1S_0$ and ${}^1S_0 \to {}^3P_0$ amplitudes. However, it would be desirable to clarify the origin of some sign and size differences for certain amplitudes. For instance, the neutron-induced contribution to the ${}^1S_0 \to {}^1S_0$ amplitude is -0.07 times the proton-induced one in ref. [64], while it is a factor -0.75 the proton-induced one in ref. [66]. The proton-induced ${}^1S_0 \to {}^3P_0$ amplitude is much larger in size in ref. [66] than the one obtained in ref. [64]. Therefore, although the results of both works are qualitatively consistent, they still show important quantitative differences.

Table 14: Quark-model results of ref. [65] for the non-mesonic decay rate and ratio Γ_n/Γ_p of light hypernuclei.

	OPE	OPE and DQ	EXP	
$\Gamma_{nm}({}^5_\Lambda\text{He})$	0.216	0.627	0.41 ± 0.14 [30]	
$\Gamma_n/\Gamma_p({}^5_\Lambda\text{He})$	0.132	0.489	0.93 ± 0.55 [30]	
$\Gamma_{nm}({}^4_\Lambda\text{He})$	0.154	0.253	0.20 ± 0.05 [81]	0.17 ± 0.05 [80]
$\Gamma_n/\Gamma_p({}^4_\Lambda\text{He})$	0.061	0.178	0.25 ± 0.13 [81]	0.06 ± 0.30 [80]

The amplitudes obtained in ref. [64] were used to determine the partial non-mesonic decay widths of s-shell nuclei but the results depended on the relative sign between the quark and the OPE contributions. Using the soft pion theorem, the authors clarified recently [65] the sign ambiguity. This theorem allows one to relate the sign of the $\Lambda \to n\pi^0$ coupling constant (relevant for the OPE mechanism) to the PC baryon-baryon transition amplitude $\Lambda \to n$, which was computed using the quark Hamiltonian and their quark model wave functions. A more realistic Λ wave function, pushed to the surface by the effect of a repulsive Λ-nucleus potential at short distances, was also used in ref. [65]. The results, summarized in Table 14, improve substantially those obtained in their previous calculations [64]. These results are promising but, before calculations of the decay of heavier hypernuclei are attempted

within this model, it would be desirable to establish the connection between the effective quark Hamiltonian and the empirical $\Lambda \to N\pi$ vertex.

3.1.4 $\Delta I = 1/2$ violation?

a) Phenomenology

Non-mesonic weak decays of light hypernuclei can be used to test the validity of the phenomenological $\Delta I = 1/2$ rule. One must first observe that, since the ΛN pair is in a $L = 0$ state, the possible transitions are those listed in Table 15.

Table 15: Possible $\Lambda N \to NN$ transitions starting from a $L = 0$ ΛN pair.

$^1S_0$	$\to$	$^1S_0$	(I=1)
	$\to$	$^3P_0$	(I=1)
$^3S_1$	$\to$	$^3S_1$	(I=0)
	$\to$	$^3D_1$	(I=0)
	$\to$	$^1P_1$	(I=0)
	$\to$	$^3P_1$	(I=1)

The neutron-induced transitions can only lead to $I = 1$ final states and, if the $\Delta I = 1/2$ rule applies, then the ratio of neutron- to proton-stimulated transitions to final $I = 1$ states must be [52]

$$\frac{\Gamma_n^{(I=1)}}{\Gamma_p^{(I=1)}} = 2 \ . \tag{44}$$

Therefore, by isolating the initial singlet spin state $^1S_0$, which leads to only $I = 1$ final states, both in neutron- and proton-induced decays, the validity of the $\Delta I = 1/2$ rule in the non-mesonic decay could be verified. This idea stimulated a large amount of experimental effort [80,81,96,97]. The connection with experiments is done following the phenomenological model of Block and Dalitz [52] and updated by Dover [98], according to which the non-mesonic decay rates of light hypernuclei are expressed in terms of elementary interaction strengths between singlet or triplet ΛN pairs:

$$\Gamma_{nm}({}^4_\Lambda\mathrm{H}) = \frac{1}{6}\rho_3(3R_{n1} + R_{n0} + 2R_{p0}) \tag{45}$$

$$\Gamma_{nm}({}^4_\Lambda\mathrm{He}) = \frac{1}{6}\rho_3(2R_{n0} + 3R_{p1} + R_{p0}) \tag{46}$$

$$\Gamma_{nm}({}^5_\Lambda\mathrm{He}) = \frac{1}{8}\rho_4(3R_{n1} + R_{n0} + 3R_{p1} + R_{p0}) \ . \tag{47}$$

The quantities R_{NS} stand for the non-mesonic decay of a ΛN pair with spin S, for unit density of nucleon N at the Λ position, and ρ_A denotes the mean nucleon density at the Λ position. An average over spin and charge is implied in eqs. (45)−(47). These expressions also assume that the final state interactions, which were shown to be important in the non-mesonic decay of the hypertriton [90], are contained in the

elementary interaction strengths and thus are the same in all these light hypernuclei. The densities cancel in forming the ratios

$$\gamma^4 = \frac{\Gamma_n(^4_\Lambda\mathrm{He})}{\Gamma_p(^4_\Lambda\mathrm{He})} = \frac{2R_{n0}}{3R_{p1}+R_{p0}} \tag{48}$$

$$\gamma^5 = \frac{\Gamma_n(^5_\Lambda\mathrm{He})}{\Gamma_p(^5_\Lambda\mathrm{He})} = \frac{3R_{n1}+R_{n0}}{3R_{p1}+R_{p0}} \tag{49}$$

$$\gamma_{nm} = \frac{\Gamma_{nm}(^4_\Lambda\mathrm{He})}{\Gamma_{nm}(^4_\Lambda\mathrm{H})} = \frac{2R_{n0}+3R_{p1}+R_{p0}}{3R_{n1}+R_{n0}+2R_{p0}} \ , \tag{50}$$

all of which involve experimentally known decay rates, as seen in Table 16, and therefore allow one to extract the ratio

$$\kappa = \frac{R_{n0}}{R_{p0}} = \frac{\gamma_{nm}\gamma^4}{1+\gamma^4-\gamma_{nm}\gamma^5} \ . \tag{51}$$

Table 16: Experimental weak decay observables of several s-shell hypernuclei.

	$^5_\Lambda$He	$^4_\Lambda$He		$^4_\Lambda$H
	[30]	[81]	[80]	[80]
Γ_n	0.20 ± 0.11	0.04 ± 0.02	0.01 ± 0.05	
Γ_p	0.21 ± 0.07	0.16 ± 0.02	0.16 ± 0.02	
Γ_n/Γ_p	0.93 ± 0.55	0.25 ± 0.13	0.06 ± 0.30	
Γ_{nm}	0.41 ± 0.14	0.20 ± 0.05	0.17 ± 0.05	0.17 ± 0.11

Taking the central values of the KEK [80] or BNL [81] experiments, the value for κ is 0.4 or 0.8 but the error bars are so large that a value of 2, compatible with the $\Delta I = 1/2$ rule, is not ruled out [97]. A much more direct determination of κ would be obtained from

$$\kappa = \frac{\Gamma_n(^4_\Lambda\mathrm{He})}{\Gamma_p(^4_\Lambda\mathrm{H})} = \frac{R_{n0}}{R_{p0}} \ , \tag{52}$$

which requires the measurement of the partial rates for $^4_\Lambda$H, an attempt that will be made in experiment E907 at BNL [81]. Since the partial neutron rate for $^4_\Lambda$He has been measured to be small, even if the error bar is large, the $\Delta I = 1/2$ rule would pose severe constraints on the value of $\Gamma_p(^4_\Lambda\mathrm{H})$, which could not exceed a few percent of the free Λ decay rate.

b) Models

The quark model of refs. [64, 66] is based on the effective 4 quark Hamiltonian with QCD corrections [94] extended down to an energy scale $\mu^2 \simeq \mu_0^2$ [95] at which $\alpha(\mu_0^2) = 1$. This quark Hamiltonian contains some enhancement of the $\Delta I = 1/2$ transitions although it is still insufficient to explain the ratio of $\Delta I = 1/2$ to $\Delta I = 3/2$ amplitudes for the non-leptonic weak decay of K, Λ and other strange hadrons. As mentioned in the previous section, two body amplitudes were evaluated by combining the quark Hamiltonian with a constituent quark model for the baryons. In spite of

the numerical differences, both models predict substantial $\Delta I = 3/2$ contributions to the spin singlet amplitudes ${}^1S_0 \to {}^1S_0$ and ${}^1S_0 \to {}^3P_0$. Therefore, these are the most important ones to measure in order to determine violations of the $\Delta I = 1/2$ rule.

In ref. [99] violation of the $\Delta I = 1/2$ rule in the $\Lambda N \to NN$ mechanism was investigated in the framework of a meson exchange model. The work is based on the observation that, while the $\Delta I = 3/2$ contributions to the weak coupling constants of baryons to the pseudoscalar mesons are empirically known to be small, this is not necessarily the case for the vector mesons. Indeed, based on the weak QCD-corrected four quark effective Hamiltonian at a scale $\simeq 1$ GeV [100], the factorization contributions to the weak $\Lambda N\rho$ and $\Sigma N\rho$ couplings were found to contain $\Delta I = 3/2$ terms comparable in magnitude to the $\Delta I = 1/2$ ones [84]. The factorization approximation in the evaluation of the $\Delta I = 3/2$ amplitudes for the known hyperon decays yields [101]: (1) good fits for the s-wave and p-wave Ξ amplitudes and the s-wave triangle discrepancy, (2) an underestimate of the p-wave Σ triangle discrepancy by a factor 3–4, and (3) an overestimate of the s-wave and p-wave Λ amplitudes by a factor 3–4. It is important to notice, however, that the experimental errors on the $\Delta I = 3/2$ amplitudes are large and the above mentioned discrepancies are within the 2σ level. The work of ref. [99] takes the predicted $\Delta I = 3/2$ contributions to the coupling constants of the vector mesons and rescales them by factors ranging in between $(-3, 3)$ to account for the limitations of the factorization model. Their $\Delta I = 1/2$ potential was extended to incorporate the $\Delta I = 3/2$ transitions of the ρ and K^* mesons by assuming the Λ to behave as a $|3/2\ -1/2>$ isospurion and replacing the isospin $\vec{\tau}\vec{\tau}$ operator in the potential by $\vec{\tau}_{3/2}\vec{\tau}$, where $\vec{\tau}_{3/2}$ is the usual isospin $3/2 \to 1/2$ transition operator. Even if the $\Delta I = 3/2$ couplings of the vector mesons were comparable in magnitude to the corresponding $\Delta I = 1/2$ ones, it was found that, when all the other mesons were incorporated, the decay rate of ${}^{12}_{\Lambda}$C changed at most by 6%, the proton-induced rate was affected at most by 10%, while the neutron-induced rate could change by up to a factor 2. In the most favorable scaling situation (a scale factor 3 for both ρ and K^*) the ratio Γ_n/Γ_p changed from the $\Delta I = 1/2$ value of 0.07 to 0.14, which is still away from the experimental values.

These findings are substantially different than those found in the quark model works [64, 66], were the $\Delta I = 3/2$ amplitudes seem to play a much more relevant role. Therefore a direct determination of the spin singlet ratio R_{n0}/R_{p0}, through the measurement of nucleon induced decays of light hypernuclei, is very much desired in order to clarify the issue of $\Delta I = 1/2$ violation in the non-mesonic weak decay.

3.2 Asymmetry

The possibility of measuring the asymmetry in the angular distribution of protons from the weak decay of polarized hypernuclei offers a unique opportunity to learn about the weak decay mechanism. The asymmetry is due to an interference between PC and PV amplitudes and, hence, can give complementary information to that obtained from total and partial rates which are dominated by the PC piece of the $\Lambda N \to NN$ interaction.

The first observation of asymmetries on the decay products from polarized hyper-

nuclei was done at KEK [73]. There, polarized hypernuclei ($^{12}_{\Lambda}\vec{\mathrm{C}}$, $^{11}_{\Lambda}\vec{\mathrm{B}}$) were created through the (π^+, K^+) reaction, which has been shown to produce nonnegligible polarization perpendicular to the reaction plane for a momentum of the pion $p_\pi \sim 1.04$ GeV/c at small K^+ scattering angles $(10 - 15^\circ)$ where the cross section is still appreciable [102, 103].

The intensity of protons emitted at an angle χ with respect to the polarization axis in the decay of polarized hypernuclei is given by

$$I(\chi) = \mathrm{Tr}(\mathcal{M}\rho\mathcal{M}^\dagger) \ , \tag{53}$$

where $\mathcal{M}$ is the hypernuclear transition operator and

$$\rho(J) = \frac{1}{2J+1}\left(1 + \frac{3}{J+1}P_y S_y\right) \tag{54}$$

is the density matrix describing the hypernucleus of spin J polarized along the y axis, which is perpendicular to the reaction plane. Eq. (53) can be written as

$$I(\chi) = I_0\left(1 + P_y A_y(\chi)\right) \ , \tag{55}$$

where I_0 is the isotropic intensity of protons from the decay of unpolarized hypernuclei and $A_y(\chi)$ the asymmetry parameter which reads

$$A_y(\chi) = \frac{3}{J+1}\frac{\mathrm{Tr}(\mathcal{M}S_y\mathcal{M}^\dagger)}{\mathrm{Tr}(\mathcal{M}\mathcal{M}^\dagger)} = \frac{3}{J+1}\frac{\sum\limits_{M_i}\sigma(M_i)M_i}{\sum\limits_{M_i}\sigma(M_i)}\cos\chi = A_y\cos\chi \tag{56}$$

The last equation shows that the asymmetry exhibits a simple $\cos\chi$ dependence and is given in terms of $\sigma(M_i)$, the weak decay probability for a hypernucleus with spin projection M_i ejecting protons along the quantization axis. The experiment compares the total number of protons emerging parallel or antiparallel to the y-axis and , therefore, the product $P_y A_y$ is determined. Using standard angular momentum algebra and assuming the Λ to couple only to the nuclear core ground state of spin J_c, one can obtain the Λ polarization as

$$p_\Lambda = \begin{cases} -\dfrac{J}{J+1}P_y & \text{if} \quad J = J_c - 1/2 \\ P_y & \text{if} \quad J = J_c + 1/2 \end{cases} \tag{57}$$

and define the intrinsic Λ asymmetry parameter

$$a_\Lambda = \begin{cases} -\dfrac{J+1}{J}A_y & \text{if} \quad J = J_c - 1/2 \\ A_y & \text{if} \quad J = J_c + 1/2 \end{cases} \tag{58}$$

such that the asymmetry

$$\mathcal{A} = P_y A_y \cos\chi = p_\Lambda a_\Lambda \cos\chi \tag{59}$$

is expressed in terms of Λ properties, p_Λ and a_Λ, which are then characteristic of the elementary $\vec{\Lambda}N \to NN$ reaction.

In order to compare with experiment, the polarization of the hypernucleus must be known. Until now this information is not available and it is necessary to resort to theoretical models, which take into account the conditions of the production reaction. Given the energy resolution of the KEK experiment [73] ($5-7$ MeV), several hypernuclear states can be excited, which then decay electromagnetically and/or by particle emission to a hypernuclear ground state prior to the weak decay. To determine the polarization at this stage one requires: i) the amount of polarization of the states excited by the production mechanism, along with their corresponding formation cross sections, and ii) an attenuation coefficient to account for the loss of polarization of each level in the deexcitation process [104].

In ref. [102] one-particle one-hole ($j_n^{-1} j_\Lambda$) hypernuclear wave functions were employed to obtain the polarizations of typical states within the p-shell region. The model was refined in [103] by incorporating configuration-mixed shell-model wave functions. Using their predictions for the three 1^- states in ${}^{12}_{\Lambda}$C and the depolarization formalism of ref. [104], one obtains $P_y = -0.19$ ($p_\Lambda = 0.095$). On the other hand, the hypernucleus ${}^{11}_{\Lambda}$B is created by particle emission from excited states of ${}^{12}_{\Lambda}$C. The window of excitation energy that spans 1.55 MeV between the (p $+{}^{11}_{\Lambda}$B) and the ($\Lambda+{}^{11}$C) particle decay threshold contains three positive-parity states: two 2^+ states separated by ~ 800 KeV and a narrow 0^+ state just below the ($\Lambda+{}^{11}$C) threshold. Using the model of ref. [103], which predicts equal formation cross sections for the 2^+_1 and 2^+_2 states, and neglecting the 0^+ state because of its relatively small cross section, a polarization of $P_y = -0.29$ ($p_\Lambda = 0.21$) is obtained. However, hypernuclear structure calculations by Auerbach et al. [105] predicted strong configuration mixing which reduced the cross section of the lower 2^+ state by a factor of three relative to the higher one. This prediction was verified by a reanalysis of older emulsion data [106]. Taking these relative weights into account, one obtains the more realistic value $P_y = -0.43$ ($p_\Lambda = 0.31$).

In Table 17 a comparison of theoretical results to the presently available data is made. The two meson exchange models predict a quite similar asymmetry parameter a_Λ which ranges between -0.3 and -0.4 for the different hypernuclei. The comparison with experiment must be made at the level of the asymmetry, for which it is necessary to multiply a_Λ by the Λ polarization discussed above. Good agreement with the data is obtained. However, the error bars are still so large that not much can be learned about the mechanism governing the decay.

In order to avoid the need for theoretical input and access A_y directly, a new experiment at KEK [107] was devised to measure the decay of polarized ${}^{5}_{\Lambda}$He, extracting both the pion asymmetry from the mesonic channel, $\mathcal{A}_{\pi^-}$, and the proton asymmetry from the non-mesonic decay, $\mathcal{A}$. The asymmetry parameter a_{π^-} of the pionic channel has been estimated to be very similar to that of the free Λ decay [108], and, therefore, the hypernuclear polarization can be obtained from the relation $P_y = \mathcal{A}_{\pi^-}/a_{\pi^-}$. Combining this value with the measured proton asymmetry $\mathcal{A}$, permits to determine the asymmetry parameter for the non-mesonic decay from the equality $A_y = \mathcal{A}/P_y$.

A preliminar analysis of this experiment has recently become available [109] and

Table 17: Proton asymmetry from the weak decay of hypernuclei.

	Parreño et al. [58]			Dubach et al. [57]
	${}^{5}_{\Lambda}$He	${}^{11}_{\Lambda}$B	${}^{12}_{\Lambda}$C	nuc. matter
a_Λ (π corr.)			-0.238	-0.192
a_Λ (all mesons)	-0.273	-0.391	-0.316	-0.443
p_Λ		0.31	0.095	
$\mathcal{A} = p_\Lambda a_\Lambda$		-0.12	-0.13	
$\mathcal{A}$ (EXP) [73]		-0.20 ± 0.10	-0.01 ± 0.10	

gives: $p_\Lambda = 0.217 \pm 0.087 \pm 0.021$ for an emerging K^+ angle $2 <| \theta_K |< 7^\circ$ and $p_\Lambda = 0.382 \pm 0.114 \pm 0.013$ for $7 <| \theta_K |< 15^\circ$. For the proton asymmetry the measured values are: $\mathcal{A} = 0.102 \pm 0.050 \pm 0.005$ for $2 <| \theta_K |< 7^\circ$ and $\mathcal{A} = 0.045 \pm 0.099 \pm 0.021$ for $7 <| \theta_K |< 15^\circ$. The combination of these preliminary results, which show large uncertainties, would give rise to a positive asymmetry parameter a_Λ, in total contradiction with their previous results [73] and the theoretical predictions shown in Table 17. One would also expect a straight line, passing through the origin, when representing the asymmetry $\mathcal{A} = p_\Lambda a_\Lambda$ as a function of p_Λ. The two new experimental points do not even show this behavior. However, one should keep in mind that corrections due to the leaking of pions into the proton identification area still need to be made [109] and, therefore, the analysis is not yet complete.

3.3 Two-nucleon induced decay

The relevance of the two-nucleon induced channel, $\Lambda NN \to NNN$, in the decay of hypernuclei was first pointed out by Alberico et al. [110]. This transition can be viewed as coming from the absorption of a virtual pion emitted in the weak vertex by two strongly correlated nucleons, as depicted schematically in fig. 14. An interesting point raised in ref. [110] was that this channel affects the emission of neutrons and could have some relevance in the experimental determination of the ratio Γ_n/Γ_p. Since pions are absorbed mainly by neutron-proton pairs, the $2N$-induced decay proceeds basically through the mode $\Lambda np \to nnp$, emitting twice as many neutrons than protons. Hence, an experimental observation of a large number of neutrons could still be compatible with a smaller value for Γ_n/Γ_p if the $2N$ mechanism was appreciably large.

In ref. [110] the decay width of a Λ in nuclear matter was calculated within the propagator method formalism discussed in Sect. 2.1.1, which allows treating all the decay channels in an unified way. Eq. (10) needs to be modified to include the effect of form factors and short-range correlations, which have been shown to be important for the $1N$-induced mechanism $\Lambda N \to NN$. Thus, a monopole form factor at both the strong and weak vertices

$$F(q) = \frac{\Lambda^2 - \mu^2}{\Lambda^2 - q^2} \ , \tag{60}$$

with $\Lambda \sim 1.2$ GeV is included. Moreover, the pion interaction between two nucleons

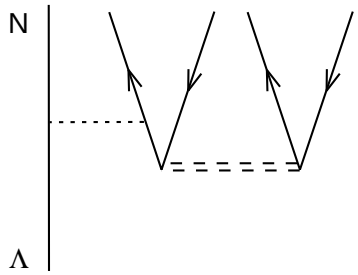

Figure 14: Schematic representation of the Λ decay coupling to 2p2h components through virtual (close to real) pion absorption.

is replaced by the particle-hole interaction of refs. [111, 112]

$$V_{ph} = \{V_L(q)\hat{q}_i\hat{q}_j + V_T(q)(\delta_{ij} - \hat{q}_i\hat{q}_j)\}\,\sigma_i\sigma_j\vec{\tau}\vec{\tau}\ , \tag{61}$$

which includes π and ρ exchange modulated by the effect of short range correlations. Detailed expressions of $V_L(q)$ and $V_T(q)$ can be found in ref. [13]. It is convenient to split $V_L(q)$ into the free pion propagator plus the Landau-Migdal parameter, g', which here is slightly momentum dependent

$$V_L(q) = \left(\frac{f}{\mu}\right)^2 \left[\vec{q}^{\,2}F^2(q)D_0(q) + g'(q)\right]\ . \tag{62}$$

The ΛN correlations are treated in a similar way as in [13] by modifying the pion exchanged between the weak and strong vertices. The decay width can be finally written as

$$\begin{aligned}\Gamma(k) &= -6(G_F\mu^2)^2 \int \frac{d^3q}{(2\pi)^3}[1 - n(\vec{k}-\vec{q})]\theta(k^0 - E(\vec{k}-\vec{q}) - V_N) \\ &\times \ \mathrm{Im}\,\alpha(q)|_{q^0 = k^0 - E(\vec{k}-\vec{q}) - V_N}\ ,\end{aligned} \tag{63}$$

with

$$\begin{aligned}\alpha(q) &= \left(S^2 + \left(\frac{P}{\mu}\right)^2 \vec{q}^{\,2}\right) F^2(q)D_0(q) \\ &+ \frac{\tilde{S}^2(q)U(q)}{1 - V_L(q)U(q)} + \frac{\tilde{P}_L^2(q)U(q)}{1 - V_L(q)U(q)} \\ &+ 2\frac{\tilde{P}_T^2(q)U(q)}{1 - V_T(q)U(q)}\ ,\end{aligned} \tag{64}$$

where the functions $\tilde{S}(q)$, $\tilde{P}_L(q)$ and $\tilde{P}_T(q)$, defined explicitly in ref. [13], reduce to

$$\tilde{S}(q) \rightarrow \left(\frac{f}{\mu}\right) S D_0(q) F^2(q) \tag{65}$$

$$\tilde{P}_L(q) \rightarrow \left(\frac{f}{\mu}\right) \frac{P}{\mu} \vec{q}^{\,2} D_0(q) F^2(q) \tag{66}$$

$$\tilde{P}_T(q) \rightarrow 0 \tag{67}$$

in the absence of ΛN short range correlations.

The $2N$-induced Λ decay mode appears when one considers the absorption of the virtual pion by 2 particle-2 hole ($2p2h$) states. Therefore, the function $U(q)$ in eq. (64) must include a term, $U_{2p2h}(q)$, that accounts for this coupling and becomes

$$U(q) = U_N(q) + U_\Delta(q) + U_{2p2h}(q) \ . \tag{68}$$

Before going into the details on how this function is determined, let us illustrate the physical mechanism that leads to the new decay channel. The strength of a free pion, which is accumulated in a delta function around a momentum value of 100 MeV/c, spreads in the medium over a wide range of energies due to the coupling of the pion to ph, Δh and $2p2h$ excitations. This distribution presents a Breit-Wigner type peak, the position of which changes slightly from the original pion pole. The energy and momentum of the pion at the peak is such that, at normal nuclear matter density, still enforces a nucleon momentum which lies below the Fermi momentum. However, the width of the distribution is such that part of its tail corresponds to a Pauli unblocked situation and, since at low pion energies this width is mostly due to pion absorption through $2p2h$ states, as shown in fig. 14, the new mode would be observed as three particle emission from $\Lambda NN \rightarrow NNN$.

In ref. [110] the following parametrization was used

$$U_{2p2h} = -4\pi \vec{q}^{\,2} \rho^2 \mathcal{C}_0 \ , \tag{69}$$

with a value $\mathrm{Im}\,\mathcal{C}_0 = 0.18\mu^{-6}$ taken from theoretical studies performed in connection with (e, e') reactions [113] and compatible with data from pionic atoms, provided the real part of $\mathcal{C}_0$ was $\mathrm{Re}\,\mathcal{C}_0 = 0.40\mu^{-6}$. The value of U_{2p2h} was taken constant, even if the phase space in the Λ decay forces one to move away from the situation in pionic atoms to values of $(q^0, \vec{q})$ different from $(\mu, \vec{0})$. Moreover, $\mathrm{Im}\,U_{2p2h}$ was set to zero in the region where $\mathrm{Im}\,U_N \neq 0$. Their results for the $2N$-induced decay rate of a Λ in nuclear matter at an average nuclear density $\rho = 0.69\rho_0$, where ρ_0 is the normal density, are shown in Table 18, splitted into the s-wave, p-wave longitudinal and p-wave transverse contributions. The final result of 0.52 represents a fraction of about 40% of the $1N$-induced decay rate.

The relative large strength of this channel and the repercussion it has in the proper interpretation of the ratio Γ_n/Γ_p motivated a more detailed analysis [67], in which a more realistic pion self-energy was used and the results were extended to finite nuclei via the LDA. The determination of U_{2p2h} was based on new developments in

Table 18: $2N$-induced contribution to the Λ decay rate in nuclear mattter.

	[110]	$\mathcal{C}_0^*$	Ph. space
S	0.40	0.119	0.148
P_L	0.079	0.023	0.026
P_T	0.040	0.023	0.065
Γ_{2p2h}	0.52	0.165	0.238

the extraction of the optical potential from pionic atoms [114], reanalyzed in ref. [115] to account for different neutron and proton radii, which yielded

$$\Pi_{2p2h}(q^0=\mu,\vec{q}\sim 0,\rho) = -4\pi\vec{q}^{\,2}\rho^2\left(1+\frac{1}{2}\varepsilon\right)^{-1}\mathcal{C}_0 \tag{70}$$

with

$$\begin{aligned}\varepsilon &= \frac{\mu}{M}\\ \mathcal{C}_0 &= (0.073+i0.068)\mu^{-6}\end{aligned}$$

However, since the propagator method model described above generates the Lorentz-Lorenz correction automatically, one needs to rewrite the information of eq. (70) accordingly. Thus, for the average density of pionic atoms in p-wave ($0.75\rho_0$ according to [116]), the results of our formulation should coincide with the experimental one given in eq. (70). This is readily obtained with the help of eq. (8) and the result for U_{2p2h} is [67]

$$\left(\frac{f}{\mu}\right)^2\vec{q}^{\,2}U_{2p2h}(q^0=\mu,\vec{q}\sim 0,\rho) = -4\pi\vec{q}^{\,2}\rho^2\mathcal{C}_0^*\ , \tag{71}$$

with

$$\mathcal{C}_0^* = (0.105+i0.096)\mu^{-6}\ , \tag{72}$$

which yields a value for $\mathrm{Im}\,\mathcal{C}_0^*$ half of that of ref. [110] and a value for $\mathrm{Re}\,\mathcal{C}_0^*$ four times smaller. The extension of the self-energy to new kinematical regions away from pionic atoms was also performed in ref. [67]. The importance of all these modifications is displayed in Table 18, where the third column corresponds to the same calculation of ref. [110] but replacing their $\mathcal{C}_0$ value by the new $\mathcal{C}_0^*$ one. The results are reduced by a factor 3 due to a smaller absorptive $\mathrm{Im}\,\mathcal{C}_0^*$ and a less attractive $\mathrm{Re}\,\Pi_{2p2h}$ which moves the pion pole to a smaller momentum. Not forcing $\mathrm{Im}\,U_{2p2h}=0$ in the ph excitation region (where $\mathrm{Im}\,U_N\neq 0$) and taking the phase-space modifications into account increase the results further, as seen in the last column of Table 18, but the final value is less than half that obtained previously [110].

Even if this decay channel turns out to be considerably smaller than claimed before, it will be shown in the next section that its consideration has repercussions in the experimental determination of the Γ_n/Γ_p ratio. This investigation requires to have predictions for the $2N$-induced decay rate of finite nuclei, which were also obtained in ref. [67] on the basis of the LDA shown in eq. (13). The results are

Table 19: Mesonic, $1N$-induced and $2N$-induced decay rates for several hypernuclei in the LDA [67].

	Γ_m	Γ_{nm}	Γ_{2p2h}
${}^{12}_{\Lambda}$C	0.31	1.45	0.27
${}^{16}_{\Lambda}$O	0.24	1.54	0.29
${}^{20}_{\Lambda}$Ne	0.14	1.60	0.32
${}^{40}_{\Lambda}$Ca	0.03	1.76	0.32
${}^{56}_{\Lambda}$Fe	0.01	1.82	0.32
${}^{89}_{\Lambda}$Y	—	1.88	0.31
${}^{208}_{\Lambda}$Pb	—	1.93	0.30

displayed in Table 19 for different hypernuclei, where, for completeness, the decay rates from the mesonic and $1N$-induced channels are also shown.

The total lifetimes —inverse of the total decay widths— are somewhat small compared with the recent lifetime measurements at KEK [117], which in the case of ${}^{56}_{\Lambda}$Fe is 215 ± 14 ps, a factor 1.8 larger than the result obtained from Table 19. However, the lifetime of ${}^{208}_{\Lambda}$Pb derived from the table is only 20% smaller than the central value $145 \pm 7 \pm 23$ ps obtained for ${}^{209}_{\Lambda}$Bi in Jülich [118] and compatible within errors. The latter measurements are done by bombarding heavy nuclei with protons and looking at the delayed fission fragments. The method was proved to work in ref. [119] and used in the experiment of ref. [118] in order to obtain the hypernuclear widths with more precission. These latter experimental results are also compatible with those of ref. [120] obtained from $\overline{p}$ interactions with nuclei which, however, have large uncertainties. One must note that the theoretical results are somewhat dependent on the ΛN correlations, controlled by the g'_Λ parameter, and on the Λ wave function used in the LDA. The $1N$-induced rate for ${}^{12}_{\Lambda}$C would be reduced from 1.45 to 1.26 if a more extended Λ wave function with an oscillator parameter $b_\Lambda = 1.87$ fm and a value $g'_\Lambda = 0.2$ were used. This value for g'_Λ is what corresponds to a Bessel type correlation function $f(r) = 1 - j_0(q_c r)$ with $q_c = 3.93$ fm^{-1}, very similar to the correlation function used in ref. [58] based on realistic ΛN wavefunctions obtained from the Nijmegen interactions. Therefore, the results in Table 19 could easily be 10-15% smaller and, correspondingly, the lifetimes 10-15% larger, which would then agree better with the very heavy hypernuclei results [118, 120] but would still be in disagreement with the KEK ones.

3.4 The Γ_n/Γ_p puzzle

As mentioned in the previous section, one of the interesting consequences of the $2N$-induced mechanism is that, since pions are absorbed predominantly by np pairs, this decay mechanism would emit two neutrons and one proton. Hence, part of the large number of observed neutrons would then come from the $2N$-induced channel and the ratio Γ_n/Γ_p would not need to be so large as what is found in the present analyses, which associate all non-mesonic decay to the $1N$-induced mechanisms. Actually, as shown in ref. [67] and summarized below, the situation is not so clear.

The experimental analysis of ref. [30] takes only the $1N$-mechanism into account and the assignment of the number of neutrons and protons goes as

$$\begin{aligned} N_n &\sim 2\Gamma_n^{\rm exp} + \Gamma_p^{\rm exp} \\ N_p &\sim \Gamma_p^{\rm exp} \end{aligned} \tag{73}$$

with $\Gamma_{nm}^{\rm exp} = \Gamma_n^{\rm exp} + \Gamma_p^{\rm exp}$. However, considering the $2N$-induced mechanism and assuming that all emitted nucleons are detected, the appropriate analysis reads

$$\begin{aligned} N_n &\sim 2\Gamma_n + \Gamma_p + 2\Gamma_{2p2h} \\ N_p &\sim \Gamma_p + \Gamma_{2p2h} \ , \end{aligned} \tag{74}$$

where the $2N$-induced decay rate Γ_{2p2h} is assumed to proceed predominantly through the $\Lambda np \to nnp$ channel.

On combining the sets of eqs. (73) and (74) one finds

$$\left(\frac{\Gamma_n}{\Gamma_p}\right) = \left(\frac{\Gamma_n^{\rm exp}}{\Gamma_p^{\rm exp}}\right) \frac{1 - \frac{1}{2}\left(\left(\frac{\Gamma_n^{\rm exp}}{\Gamma_p^{\rm exp}}\right)^{-1} + 1\right)\frac{\Gamma_{2p2h}}{\Gamma_{nm}^{\rm exp}}}{1 - \left(\frac{\Gamma_n^{\rm exp}}{\Gamma_p^{\rm exp}} + 1\right)\frac{\Gamma_{2p2h}}{\Gamma_{nm}^{\rm exp}}} \ , \tag{75}$$

which gives the new ratio in terms of the old one and the $2N$-induced decay rate. From eq. (75) one can see that if $\frac{\Gamma_n^{\rm exp}}{\Gamma_p^{\rm exp}} > 0.5$, as is the case of almost all experimental results, then the ratio Γ_n/Γ_p of the new analysis is even larger, in stronger disagreement with the present theories. Taking as an example the data of ref. [30] for ${}^{12}_{\Lambda}$C, corrected for final state interactions [121], one extracts $\frac{\Gamma_n^{\rm exp}}{\Gamma_p^{\rm exp}} = 1.04$ while the new analysis gives $\frac{\Gamma_n}{\Gamma_p} = 1.54$ which shows that, even if these values have big error bars tied to the uncertainties in N_n and N_p, the $2N$-induced decay channel is relevant and needs to be considered in any experimental analysis from where the ratio Γ_n/Γ_p is to be extracted.

Note, however, that not all the three nucleons emitted in the $2N$-induced decay are necessarily fast ones [122]. If the process receives most contributions when the pion is emitted close to on shell, then the nucleon at the Λ vertex will be slow and will not be detected due to the experimental energy tresholds of around $30-40$ MeV. Assuming this to be the case, the experimental reanalysis gives, instead of the relation in eq. (75), the following one

$$\left(\frac{\Gamma_n}{\Gamma_p}\right) = \left(\frac{\Gamma_n^{\rm exp}}{\Gamma_p^{\rm exp}}\right) \frac{1 - \frac{2}{3}\left(\left(\frac{\Gamma_n^{\rm exp}}{\Gamma_p^{\rm exp}}\right)^{-1} + 1\right)\frac{\Gamma_{2p2h}}{\Gamma_{nm}}}{1 - \frac{1}{3}\left(\frac{\Gamma_n^{\rm exp}}{\Gamma_p^{\rm exp}} + 1\right)\frac{\Gamma_{2p2h}}{\Gamma_{nm}}} \ , \tag{76}$$

with $\Gamma_{nm} = \Gamma_n + \Gamma_p + \Gamma_{2p2h}$, which yields $\frac{\Gamma_n}{\Gamma_p} < \frac{\Gamma_n^{\rm exp}}{\Gamma_p^{\rm exp}}$ as long as $\frac{\Gamma_n^{\rm exp}}{\Gamma_p^{\rm exp}} < 2$.

These considerations lead to the conclusion that, in order to establish the effect of the $2N$-induced decay mode on the ratio Γ_n/Γ_p, sensitive to the detection thresholds, it is necessary to know the spectrum of the emitted nucleons from the different mechanisms. This is discussed in the next section.

3.5 Nucleon spectra

The findings of the preceding section evidence the need for theoretical calculations of the energy distribution of nucleons from the different weak decay mechanisms. These models will also have to address the problem of final state interactions of the nucleons on their way out of the nucleus.

The spectra of neutrons and protons from the weak decay of hypernuclei have been calculated in a recent work [123], taking Γ_n/Γ_p as a free parameter in order to facilitate the extraction of this ratio from the experimental data. The spectra were obtained using the propagator method formalism [13, 67] to determine the primary emitted nucleons for a given hypernucleus via the LDA, an approximation particularly suited to treat the final state interactions, as we shall see. Let us recall that the rate for a particular channel ($i = n, p, 2N$) is given by

$$\Gamma_i = \int d^3k \tilde{\rho}(\vec{k}) \Gamma_i(\vec{k}) = \int d^3k \tilde{\rho}(\vec{k}) \int d^3r \mid \phi_\Lambda(\vec{r}) \mid^2 \Gamma_i(\vec{k}, \rho(\vec{r})) \ , \tag{77}$$

where $\Gamma_i(\vec{k}, \rho(\vec{r}))$ is the decay rate of a Λ of momentum $\vec{k}$ in nuclear matter of density $\rho(\vec{r})$, which is the nuclear density at point $\vec{r}$ where the decay occurs. The function $\phi_\Lambda(\vec{r})$ is the Λ wave function at that point and an average over the Λ momentum distribution is also implied in eq. (77). The structure of the integrals involved is then

$$\Gamma_i = \int d^3k \int d^3r \int d^3q \ldots \mathrm{Im}\, U_i(q^0 = k^0 - E(\vec{k} - \vec{q}) - V_N, \vec{q}) \tag{78}$$

where the function U_i associated to the particular decay mechanism can be further decomposed in terms of the momentum variables of the emitted nucleons, as explained in ref. [123]. Then, a Monte Carlo integration method can be used to perform the integrals, where the random configurations are generated such that: i) give the relative amount of one-nucleon- and two-nucleon-induced decay probabilities according to the model described in Sect. 3.3, and ii) give the relative amount of neutron- and proton-induced decay rates, according to the input value of Γ_n/Γ_p, used as a parameter of the calculation.

In this way, each configuration determines, at each point $\vec{r}$, a number of primary emitted nucleons and their corresponding momenta. The fate of these nucleons on their way out of the nucleus is then followed using a Monte Carlo simulation method [77], which allows the nucleons to undergo collisions with other nucleons according to NN cross sections modified by Pauli blocking. In each collision, the nucleons change energy, direction and, eventually, charge, as well as exciting other nucleons above the local Fermi momentum. Then, the propagation of these secondary unbound nucleons through the nucleus is also followed.

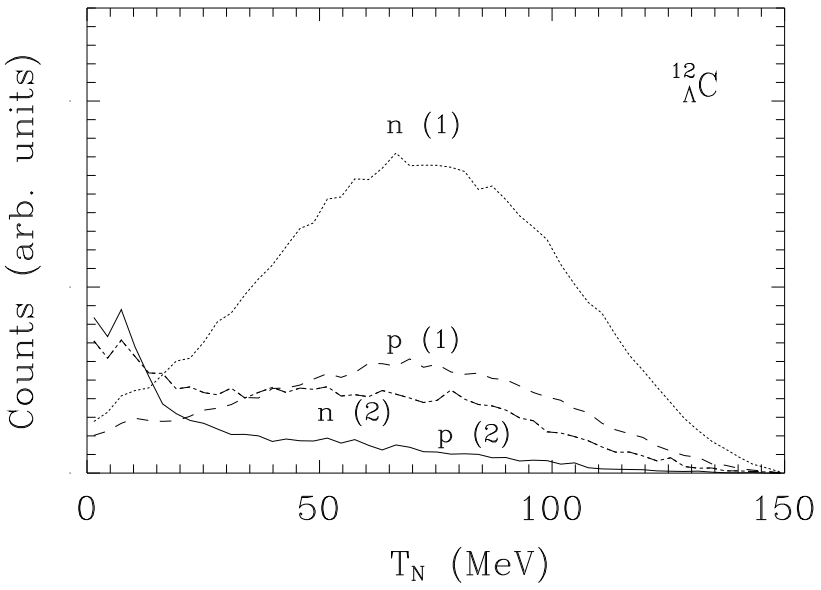

Figure 15: Spectra of neutrons and protons in the decay of $^{12}_{\Lambda}$C, assuming a ratio $\Gamma_n/\Gamma_p = 1$. Dashed line: protons from $1N$-induced decay. Dotted line: neutrons from $1N$-induced decay. Solid line: protons from $2N$-induced decay. Dash-dotted line: neutrons from $2N$-induced decay.

The obtained spectra of neutrons and protons coming from the $1N$- and $2N$-induced mechanisms in the decay of $^{12}_{\Lambda}$C are shown in fig. 15 for a value $\Gamma_n/\Gamma_p = 1$. One observes that the distribution of protons (and neutrons) from the $1N$-induced mechanism peaks around $70 - 75$ MeV, which corresponds to the energy of the most probable kinematics in which the two nucleons emerge back-to-back. The energy distribution generated by to the $2N$-induced process is flatter and presents a peak at low excitation energies, which contains mainly slow nucleons coming from the Λ vertex plus some nucleons whose energy has been degraded by the effect of final state interactions. It is clear then that the experimental thresholds ($30 - 40$ MeV) will prevent these $2N$-induced nucleons from being detected. However, a considerable fraction still leaks into the region where most $1N$-induced decay nucleons appear. Hence, separating the nucleons from both mechanisms will be very difficult, unless angular correlation measurements are also conducted. This effort is presently being carried out at Brookhaven and it is certainly encouraging to see that their preliminary results [81] already show how the back-to-back kinematics nicely selects the nucleons emitted in the $1N$-mechanism and, therefore, a cleaner extraction of the ratio Γ_n/Γ_p might soon become available.

Qualitatively similar spectrum shapes were obtained for $^{5}_{\Lambda}$He in ref. [124], where the $2N$-induced mechanism was assumed to proceed via a Δ-excited intermediate

state, although the medium modification of the Δ and other important $2p2h$ mechanisms were ignored. Final state interactions were not considered, which is reasonable for the light hypernucleus treated but does not allow one to apply the model to heavier hypernuclei.

It is clear that the spectra shown in fig. 15 would certainly differ if other values of the ratio Γ_n/Γ_p were used. A comparison of the available experimental proton spectra [30, 82] with the calculated ones for several values of Γ_n/Γ_p was also done in ref. [123] and it was found that values of $\Gamma_n/\Gamma_p \sim 2-3$ were favored, in strong contradiction with the OPE models.

However, in the same work, other observables that were less sensitive to the specific details of the Monte Carlo simulation determining the final shape of the spectrum were also studied as functions of Γ_n/Γ_p, which would probably lead to a more reliable determination of this ratio. By integrating over the energy spectra, the total number of neutrons, N_n, and protons, N_p, and therefore the ratio N_n/N_p was plotted against Γ_n/Γ_p. The experimental values of ref. [30], corrected in ref. [121], give $N_n/N_p = (2530 \pm 1050)/(1112 \pm 130)$. The error band in N_n/N_p allowed values for Γ_n/Γ_p in the range $0.0 - 1.65$ [123], perfectly compatible with the OPE predictions. Note that the inclusion of the $2N$-induced channel extended the possible values for Γ_n/Γ_p at both ends of the interval, with respect to what would have been obtained omitting this channel.

The fact that the relative error of N_n/N_p is the sum of the relative errors of N_n and N_p, together with the fact that neutrons are measured with little precision, makes the uncertainty on N_n/N_p very large and therefore leads to a poor determination of Γ_n/Γ_p. It was pointed out in ref. [123] that the separate measurement of the number of protons and neutrons per decay event, n_p and n_n, would provide more reliable predictions. As an example, fig. 16 shows the number of protons (upper half) and neutrons (lower half) per decay event for different energy cut-offs (from top to bottom: 0, 30 and 40 MeV) in the decay of ${}^{208}_{\Lambda}$Pb. If one considers a hypothetical situation in which the values of n_p and n_n could be measured with 10% accuracy and the value of Γ_n/Γ_p was around 1, then this would imply having measured values of $n_p = 0.37 \pm 10\%$ and $n_n = 1.03 \pm 10\%$, assuming an energy cut-off of 40 MeV. Representing these values in the figure and translating their error bands into the corresponding ones for Γ_n/Γ_p, one would obtain, from n_p, the value $\Gamma_n/\Gamma_p = 1.0^{+0.35}_{-0.22}$ and, from n_n, the value $\Gamma_n/\Gamma_p = 1.0^{+1.0}_{-0.52}$. This example clearly demostrates that the measurement of n_p is, so far, the most crucial one in order to determine the ratio Γ_n/Γ_p. An experimental set up to be used at TJNAF and at the Yerevan Electron Synchroton (YESS) facility has already been devised in order to measure n_p from the delayed fission events from the decay of heavy hypernuclei [125], which hopefully will lead to a cleaner determination of the ratio Γ_n/Γ_p.

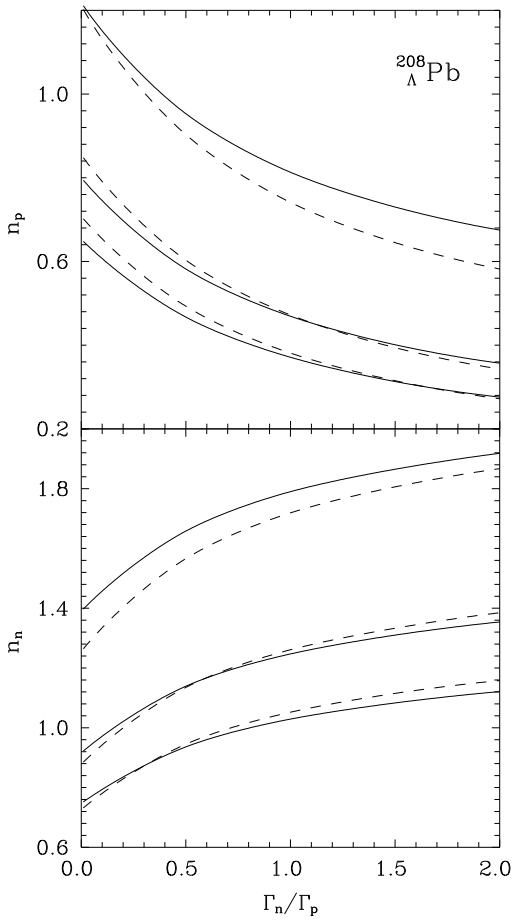

Figure 16: Number of protons (n_p) and neutrons (n_n) per Λ decay event in $^{208}_{\Lambda}$Pb. From top to bottom the results include energy cuts of 0, 30 and 40 MeV. Dashed lines: $1N$- induced mechanism. Solid lines: $1N + 2N$ mechanisms.

4 Conclusions and perspective

The discussions along this review have shown some interesting features that we summarize here.

The mesonic decay of Λ hypernuclei has offered some evidence of the strong repulsion at short distances of the ΛN interaction which appears naturally in current models of the YN interaction. The sensitivity of the mesonic decay to the pion nucleus interaction has been stressed repeatedly in the calculations. The total mesonic decay rate is appreciably enhanced due to the p-wave attraction of the optical potential. However, exclusive mesonic decay into particular final nuclear states may select the s-wave part and the partial rate can be reduced, particularly if the final nucleus is a closed shell one. Thus, investigations on Λ mesonic decay into different channels can offer complementary information on the pion nucleus optical potential and should help in deciding between different parametrizations of theoretical models, which are equally successful in explaining pion nuclear scattering or pionic atoms data. Moreover, the mesonic decay rates of heavy hypernuclei, even if small, would be most welcome since the pion renormalization is most important there. It should also be stressed that these measurements would also provide information about the π^0 nuclear interaction which is not available from scattering data.

The non-mesonic decay has been the object of intensive theoretical investigations and models going beyond the traditional one pion exchange mechanism are now available. Yet, the inclusion of heavier mesons or multimeson exchange does not change appreciably neither the decay rate nor the ratio Γ_n/Γ_p, which was the main motivation to develop such models. The incorporation of quark degrees of freedom into the picture brings interesting new features, such as important $\Delta I = 3/2$ contributions to the decay rate and the possibility of obtaining increased values for the Γ_n/Γ_p ratio. However, more theoretical investigations are needed to understand both the mesonic and the non-mesonic decays from the same basic quark Hamiltonian. Although the discrepancy between the theoretical models and experiment for the value of Γ_n/Γ_p is still a puzzle, one must note that the experimental uncertainties for this ratio are very large. The two-nucleon induced decay was proposed as a hope to resolve this puzzle but, as discussed here, the consideration of this channel leads to enlarged error bars in the experimental analysis. Nevertheless, some efficient methods to determine Γ_n/Γ_p with far more precision than has been possible until now have been proposed. One possibility is through the determination of the number of protons per Λ decay and their spectra. New experiments along these lines are now planned and most awaited. Another interesting feasible experiment is the measurement in coincidence of two nucleons emerging back-to-back. This should allow to disentangle the nucleons of the one-nucleon-induced mechanism from those of the two-nucleon-induced one, leading to a cleaner determination of the Γ_n/Γ_p ratio.

Measurements of the lifetime of heavy hypernuclei are now available from different experiments and, although agreeing at the qualitative level, more precise determinations of these rates would be also helpful to establish clearly when saturation is reached and, therefore, obtain information on the range of the weak $\Lambda N \to NN$ transition.

The $\Delta I = 1/2$ violation in the non-mesonic weak decay of hypernuclei is an

intriguing possibility that should be explored further through ratios of partial decay rates of light hypernuclei.

The possibility of producing polarized hypernuclei with the (π^+, K^+) reaction has extended the available observables to asymmetries of the weak decay products. These results bring complementary information to that obtained from partial and total non-mesonic decay rates of hypernuclei and some theoretical models have now predictions for the asymmetry of the emitted particles. However, in order to constrain these models, it is necessary to reduce the experimental uncertainties and clarify the contradicting experimental results.

In summary, the field of Λ hypernuclei and their weak decay modes has experienced an impressive progress in the last decade. The availability of new data from practically all intermediate energy experimental facilities is building up the grounds for a bright future in which one may expect to settle the present problems and open the door to novel an interesting physics.

Acknowledgements

This work has been partially supported by DGICYT contracts PB95-1249 and PB96-0753, and by the E.U. contract CHRX-CT93-0323.

We would like to thank our colleagues C. Bennhold, A. Faessler, P. Fernández de Córdoba, C. García-Recio, J. Nieves, A. Parreño, L.L. Salcedo, U. Straub and M.J. Vicente-Vacas, who collaborated in obtaining many of the results reported here.

References

[1] A. Gal, Adv. Nucl. Sci. **8** (1977) 1.

[2] B. Povh, Ann. Rev. Nucl. Part. Sci. **28** (1978) 1.

[3] H. Bandō, K. Ikeda, T. Motoba, Y. Yamada and T. Yamamoto, Prog. Theor. Phys. Suppl. **81** (1985).

[4] C.B. Dover, D.J. Millener and A. Gal, Phys. Rep. **184** (1989) 1.

[5] E. Oset, P. Fernández de Córdoba, L.L. Salcedo and R. Brockmann, Phys. Reports **188** (1990) 79.

[6] J. Cohen, Prog. Part. Nucl. Phys. **25** (Pergamon, 1990) 139.

[7] H. Bandō, T. Motoba, and J. Žofka, Int. J. Mod. Phys. **A5** (1990) 4021.

[8] H. Bandō, T. Motoba, and J. Žofka, Perspectives in Meson Science, ch. 20, Eds. T. Yamazaki, K. Nakai and K. Nagamine (North Holland, 1992) 571.

[9] Prog. Theor. Phys. Suppl. **117**, Eds. T. Motoba, Y. Akaishi and K. Ikeda (1994).

[10] B.F. Gibson and E.V. Hungerford, Phys. Rep. **257** (1995) 349.

[11] Y. Akaishi and T. Yamazaki, Prog. Part. Nucl. Phys. **39** (Pergamon, 1997) 565.

[12] T. Nagae et al., Phys. Rev. Lett. **80** (1998) 1605.

[13] E. Oset and L.L. Salcedo, Nucl. Phys. **A443** (1985) 704.

[14] E. Oset and L.L. Salcedo, Nucl. Phys. **A450** (1986) 371c.

[15] K. Itonaga, T. Motoba and H. Bandō, Z. Phys. **A330** (1988) 209.

[16] T. Motoba, K. Itonaga and H. Bandō, Nucl. Phys. **A489** (1988) 683.

[17] T. Motoba, Nucl. Phys. **A527** (1991) 485c; Few Body Systems Suppl. **5** (1992) 386; Proc. Int. Symp. on Hypernuclear and Strange Particle Physics, Shimoda, 1991 [Nucl. Phys. **A547** (1992) 115c].

[18] E. Oset, P. Fernández de Córdoba, J. Nieves, A. Ramos and L.L. Salcedo, Prog. Theor. Phys. Suppl. **117** (1994) 461.

[19] H. Bandō and H. Takaki, Phys. Lett. **B150** (1985) 409.

[20] S. Fantoni and V.R. Pandharipande, Nucl. Phys. **A427** (1984) 473.

[21] P. Fernández de Córdoba and E. Oset, Nucl. Phys. **A528** (1991) 736.

[22] C. García-Recio, J. Nieves and E. Oset, Phys. Rev. **C51** (1995) 237.

[23] S.V. Akulinichev, Phys. Rev. Lett. **68** (1992) 290.

[24] M.F. Jiang and D.S. Koltun, Phys. Rev. **C46** (1992) 2462.

[25] P. Fernández de Córdoba, E. Marco, H. Muther, E. Oset and A. Faessler, Nucl. Phys. **A611** (1996) 514.

[26] A. C. Benvenuti et al., Z. Phys. **C63** (1994) 29.

[27] R. Grace et al., Phys. Rev. Lett. **55** (1985) 1055.

[28] A. Sakaguchi et al., Nuovo Cimento **102A** (1989) 511.

[29] P.D. Barnes, Nucl. Phys. **A450** (1986) 43c; **A478** (1988) 127c.

[30] J.J. Szymanski et al., Phys. Rev. **C43** (1991) 849.

[31] A. Sakaguchi et al., Phys. Rev. **C43** (1991) 73.

[32] J. Nieves and E. Oset, Phys. Rev. **C47** (1993) 1478.

[33] J. Nieves, E. Oset and C. García-Recio, Nucl. Phys. **A554** (1993) 509; *ibid.* pag. 554.

[34] Y. Kurihara, Y. Akaishi and H. Tanaka, Phys Rev. **C31** (1985) 971.

[35] E. Oset, L.L. Salcedo and Q.N. Usmani, Nucl. Phys. **A450** (1986) 67c.

[36] U. Straub, Z.Y. Zhang, K. Bräuer, A. Faessler, S.B. Khadkikar and G. Lübeck, Nucl. Phys. **A508** (1990) 385c.

[37] U. Straub, J. Nieves, A. Faessler and E. Oset. Nucl. Phys. **A556** (1993) 531.

[38] T. Motoba, H. Bandō, T. Fukuda and J. Zŏfka, Nucl. Phys. **A534** (1991) 597.

[39] Y. Yamamoto and H. Bandō, Prog. Theor. Phys. **73** (1985) 905; Prog. Theor. Phys. Suppl. **81** (1985) ch. II.

[40] I. Kumagai-Fuse, S. Okabe and Y. Akaishi, Phys. Lett. **B345** (1995) 386.

[41] Y. Kurihara, Y. Akaishi and H. Tanaka, Prog. Theor. Phys. **67** (1982) 1483.

[42] N. G. Kelkar, Mod. Phys. Lett. **A12** (1997) 511.

[43] H. Kamada, J. Golak, K. Miyagawa, H. Witala and W. Glöckle, Phys. Rev. **C** (in press). nucl-th/9709035.

[44] G. Keyes et al, Phys. Rev. **D1** (1970) 66; Phys. Rev. Lett. **20** (1968) 819; Nucl. Phys. **B67** (1973) 269.

[45] R.H. Dalitz and F. von Hippel, Nuovo Cimento **34** (1964) 799.

[46] A. Cieplý and A. Gal, Phys. Rev. **C55** (1997) 2715.

[47] B.F. Gibson and R.G.E. Timmermans, nucl-th/9711054.

[48] G. Keyes, J. Sacton, J.H. Wickens and M.M. Block, Nuovo Cim. **31A** (1976) 401.

[49] M. Oka, nucl-th/9711049.

[50] T. Kishimoto, *Weak and Electromagnetic Interactions in Nuclei*, edited by H. Ejiri, T. Kishimoto and T. Sato (World Scientific, Singapore, 1995) 514.

[51] J. Haidenbauer, K. Holinde, K. Kilian and T. Sefzick, Phys. Rev. **C52** (1995) 3496.

[52] M.M. Block and R.H. Dalitz, Phys. Rev. Lett. **11** (1963) 96; R.H. Dalitz and G. Rajasekharan, Phys. Lett. **1** (1962) 58.

[53] J.B. Adams, Phys. Rev. **156** (1967) 1611.

[54] B.H.J. McKellar and B.F. Gibson, Phys. Rev. **C30** (1984) 322.

[55] K. Takeuchi, H. Takaki, and H. Bandō, Prog. Theor. Phys. **73** (1985) 841.

[56] J.F. Dubach, Nucl. Phys. **A450** (1986) 71c.

[57] J.F. Dubach, G.B. Feldman, B.R. Holstein, L. de la Torre, Ann. Phys. (N.Y.) **249** (1996) 146.

[58] A. Parreño, A. Ramos, and C. Bennhold, Phys. Rev. **C56** (1997) 339.

[59] M. Shmatikov, Phys. Lett. **B322** (1994) 311.

[60] M. Shmatikov, Nucl. Phys. **A580** (1994) 538.

[61] K. Itonaga, T. Ueda, and T. Motoba, Nucl. Phys. **A585** (1995) 331c; *ibid.*, *Weak and Electromagnetic Interactions in Nuclei*, edited by H. Ejiri, T. Kishimoto and T. Sato (World Scientific, Singapore, 1995) 546.

[62] K. Itonaga, Proceedings of the *International Conference on Hypernuclear and Strange Particle Physics*, edited by R.E. Chrien and D.J. Millener, Nucl. Phys. **A** (in press).

[63] C.-Y. Cheung, D.P. Heddle and L.S. Kisslinger, Phys. Rev. **C27** (1983) 335; D.P. Heddle and L.S. Kisslinger, Phys. Rev. **C33**, (1986) 608.

[64] T. Inoue, S. Takeuchi, and M. Oka, Nucl. Phys. **A597** (1996) 563.

[65] T. Inoue, M. Oka, T. Motoba and K. Itonaga, Nucl. Phys. **A**, in press. nucl-th/9708041.

[66] K. Maltman and M. Shmatikov, Phys. Lett. **B331** (1994) 1.

[67] A. Ramos, E. Oset and L.L Salcedo, Phys. Rev. **C50** (1994) 2314.

[68] P. Fernández de Córdoba, E. Oset, M.J. Vicente-Vacas, Yu. Ratis, J. Nieves, B. López-Alvaredo and F. Gareev, Nucl. Phys. **A586** (1995) 586.

[69] A. Ramos, C. Bennhold, E. van Meijgaard, and B.K. Jennings, Phys. Lett. **B264** (1991) 233.

[70] A. Ramos, E. van Meijgaard, C. Bennhold and B.K. Jennings, Nucl. Phys. **A544** (1992) 703.

[71] A. Parreño, A. Ramos, and E. Oset, Phys. Rev. **C51** (1995) 2477.

[72] H. Noumi et al., Phys. Rev. **C52** (1995) 2936.

[73] S. Ajimura et al., Phys. Lett. **B282** (1992) 293.

[74] A. Parreño, A. Ramos, C. Bennhold, and D. Halderson, in *Dynamical Features of Nuclei and Finite Fermi Systems*, edited by X. Viñas, M. Pi and A. Ramos, (World Scientific, Singapore, 1994) 318.

[75] A. Parreño, Thesis, Univ. of Barcelona, 1997.

[76] V.G. Stoks, R.A.M. Klomp, C.P.F. Terheggen and J.J. de Swart, Phys. Rev. **C49** (1994) 2950.

[77] R.C. Carrasco, M.J. Vicente Vacas and E. Oset, Nucl. Phys. **A570** (1994) 701.

[78] C. Bennhold and A. Ramos, Phys. Rev. **C45** (1992) 3017.

[79] J.F. Dubach, in *Weak and Electromagnetic Interactions in Nuclei, Heidelberg, 1986*, edited by H.V. Klapdor (Springer-Verlag, Berlin, 1986) 576.

[80] H. Outa, *Weak and Electromagnetic Interactions in Nuclei*, edited by H. Ejiri, T. Kishimoto and T. Sato (World Scientific, Singapore, 1995) 532; Proceedings of the *International Conference on Hypernuclear and Strange Particle Physics*, edited by R.E. Chrien and D.J. Millener, Nucl. Phys. **A** (in press).

[81] V. Zeps, Proceedings of the *International Conference on Hypernuclear and Strange Particle Physics*, edited by R.E. Chrien and D.J. Millener, Nucl. Phys. **A** (in press).

[82] A. Montwill et al., Nucl. Phys. **A234** (1974) 413.

[83] G. Nardulli, Phys. Rev. **C38** (1988) 32.

[84] K. Maltman and M. Shmatikov, Phys. Rev. **C51** (1995) 1576.

[85] J.F. Donoghue et al., Phys. Rep. **131** (1986) 319.

[86] A. Parreño, A. Ramos, and C. Bennhold, Phys. Rev. **C52**, (1995) R1768. Erratum: *ibid.* **54** (1996) 1500.

[87] M.N. Nagels, T.A. Rijken, and J.J. de Swart, Phys. Rev. **D12** (1975) 744; **D15** (1977) 2547; **D20** (1979) 1633; P.M.M. Maessen, Th. A. Rijken and J.J. de Swart, Phys. Rev. **C40** (1989) 2226.

[88] B. Holzenkamp, K. Holinde, and J. Speth, Nucl. Phys. **A500** (1989) 485.

[89] M.J. Savage and R.P. Springer, Phys. Rev. **C53** (1996) 441. Erratum: *ibid.* **54** (1996) 2786.

[90] J. Golak, K. Miyagawa, H. Kamada, H. Witala, W. Glöckle, A. Parreño, A. Ramos, and C. Bennhold, Phys. Rev. **C55** (1997) 2196. Erratum: *ibid.* **55** (1997) 2892.

[91] K. Miyagawa, H. Kamada, W. Glöckle, and V.G.J. Stoks, Phys. Rev. **C51** (1995) 2905.

[92] C. Bennhold, A. Ramos, D.A. Aruliah, and U. Oelfke, Phys. Rev. **C45** (1992) 947.

[93] H. Bandō, Y. Shono and H. Takaki, Int. J. Mod. Phys. **A3** (1988) 1581.

[94] F.J. Gilman and M.B. Wise, Phys. Rev. **D20** (1979) 2382.

[95] E. A. Paschos, T. Schneider and Y.L. Wu, Nucl. Phys. **B332** (1990) 285.

[96] R.A. Schumacher, Nucl. Phys. **A 547** (1992) 143c, and in *Proceedings of the U.S.-Japan Seminar on the Properties and Interactions of Hyperons, Maui, HI, 1993*, edited by B.F. Gibson, P.D. Barnes and K. Nakai, (World Scientific, Singapore, 1994) 85.

[97] B. Quinn et al., *Weak and Electromagnetic Interactions in Nuclei*, edited by H. Ejiri, T. Kishimoto and T. Sato (World Scientific, Singapore, 1995) 522.

[98] C.B. Dover, Few-Body Systems Suppl. **2** (1987) 77.

[99] A. Parreño, A. Ramos, C. Bennhold, and K. Maltman, Proceedings of the *International Conference on Hypernuclear and Strange Particle Physics*, edited by R.E. Chrien and D.J. Millener, Nucl. Phys. **A** (in press). nucl-th/9712045.

[100] J.F. Donoghue, E. Golowich and B.R. Holstein, Dynamics of the Standard Model (Cambridge Univ. Press, New York, 1992).

[101] K. Maltman and M. Shmatikov, Phys. Lett. **B345** (1995) 541.

[102] H. Bandō, T. Motoba, M. Sotona, and J. Žofka, Phys. Rev. **C39**(1989) 587.

[103] K. Itonaga, T. Motoba, O. Richter and M. Sotona, Phys. Rev. **C49** (1994) 1045.

[104] H. Ejiri, T. Kishimoto and H. Noumi, Phys. Lett. **B225** (1989) 35.

[105] E. H. Auerbach, A.J. Baltz, C.B. Dover, A. Gal, S.H. Kahana, L. Ludeking, and D.J. Millener, Ann. of Phys. (N.Y.) **148** (1983) 381.

[106] R.H. Dalitz, D.H. Davies and D.N. Tovee, Nucl. Phys. **A450** (1986) 311c.

[107] T. Kishimoto, Nucl. Phys. **A585** (1995) 205c.

[108] T. Motoba and K. Itonaga, Nucl. Phys. **A577** (1994) 293c.

[109] S. Ajimura, Proceedings of the *International Conference on Hypernuclear and Strange Particle Physics*, edited by R.E. Chrien and D.J. Millener, Nucl. Phys. **A** (in press).

[110] W.M. Alberico, A. De Pace, M. Ericson and A. Molinari, Phys. Lett. **B256** (1991) 134.

[111] E. Oset and W. Weise, Nucl. Phys. **A 319** (1979) 477.

[112] E. Oset, H. Toki and W. Weise, Phys. Reports **83** (1982) 281.

[113] W.M. Alberico, M. Ericson, and A. Molinari, Ann. Phys. (NY) **154** (198) 356.

[114] O. Meirav, E. Friedman, R.R. Johnson, R. Olszewski, and P. Weber, Phys. Rev. **C40** (1989) 843.

[115] C. García-Recio, J. Nieves, and E. Oset, Nucl. Phys. **A547** (1992) 473.

[116] R. Seki and K. Masutani, Phys. Rev. **C27** (1983) 2799.

[117] H.C. Bhang, Proceedings of the *International Conference on Hypernuclear and Strange Particle Physics*, edited by R.E. Chrien and D.J. Millener, Nucl. Phys. **A** (in press).

[118] O. Schult, Proceedings of the *International Conference on Hypernuclear and Strange Particle Physics*, edited by R.E. Chrien and D.J. Millener, Nucl. Phys. **A** (in press).

[119] H. Ohm et al., Phys. Rev. **C55** (1997) 3062.

[120] T.A. Armstrong et al., Phys. Rev. **C47** (1993) 1957.

[121] G. Franklin, private communication.

[122] A. Gal, *Weak and Electromagnetic Interactions in Nuclei*, edited by H. Ejiri, T. Kishimoto and T. Sato (World Scientific, Singapore, 1995) 573.

[123] A. Ramos, M.J. Vicente-Vacas and E. Oset, Phys. Rev. **C55** (1997) 735.

[124] S. Shinmura, Prog. Theor. Phys. **97** (1997) 283.

[125] G. Bayatyan et al., Proceedings of the *International Conference on Hypernuclear and Strange Particle Physics*, edited by R.E. Chrien and D.J. Millener, Nucl. Phys. **A** (in press).